Spatial Correlations of Underground Pipeline Damage in Christchurch

Correlations with liquefaction-induced ground surface deformations and CPT-based liquefaction vulnerability index parameters

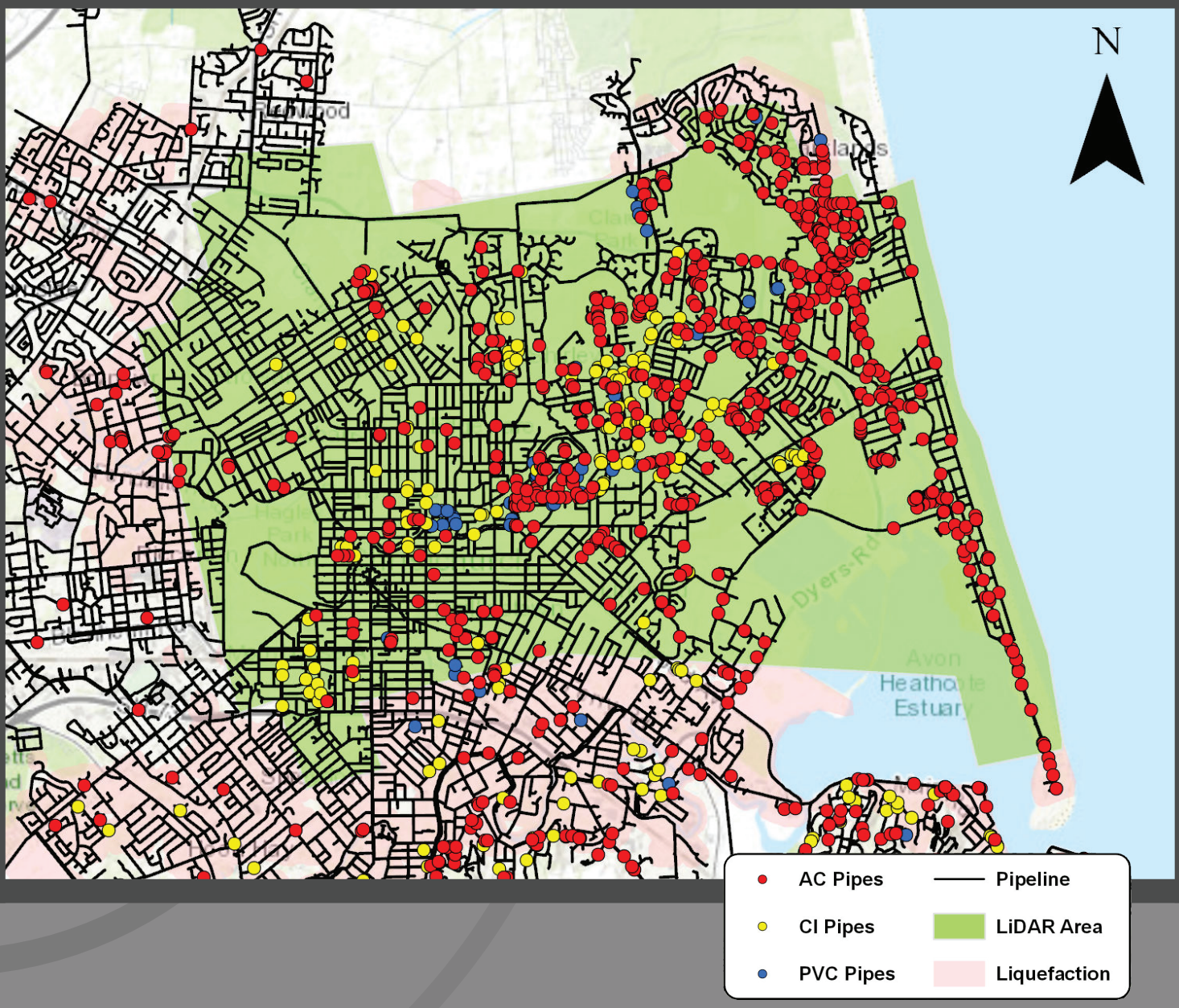

www.quakecentre.co.nz

Spatial Correlations of Underground Pipeline Damage in Christchurch

Correlations with liquefaction-induced ground surface deformations and CPT-based liquefaction vulnerability index parameters

Prepared by:

Dr. Dimitra Bouziou	Cornell University / GEK TERNA
Dr. Sjoerd van Ballegooy	Tonkin + Taylor
Dr. Luke Storie	Tonkin + Taylor
Prof. Thomas O'Rourke	Cornell University

April 2019

Cornell University

Tonkin+Taylor

Applicability

This report has been prepared for the UC Quake Centre as a technical report, with respect to the particular brief given. It is intended to inform and assist industry in the particular field and is presented without prejudice. This report is based on data provided by Christchurch City Council and data available from the New Zealand Geotechnical Database. The authors and their associated institutions/companies present this report for open consideration and future application, and do not accept liability for the application of this report's findings. Parties utilising the findings and methodologies described herein should exercise professional discretion.

Executive Summary

The 2010-2011 Canterbury Earthquake Sequence (CES) caused extreme and widespread damage to the 3 waters pipe network of Christchurch, New Zealand. Most of this damage was caused by liquefaction and lateral spreading. Researchers and practitioners have learnt many lessons in assessing liquefaction damage from these experiences. This report develops tools to assess the potential for pipeline damage based on correlations with liquefaction-induced ground movement and CPT-based liquefaction metrics. The correlations can be used for pre-event estimates as well as post-event rapid triage of pipe damage. Key inputs to the assessment are pre- and post-event LiDAR surveys; satellite imagery; CPT-based assessments of liquefaction vulnerability and Peak Ground Velocity (PGV).

The report explains how the data sets were collated and analysed to develop functions for pipe repair rates expressed in breaks per kilometre of pipeline. These repair rates cannot predict specific damage. Rather they can identify areas where damage is more likely to occur and areas where it is less likely to occur, and provide an expected damage rate (in breaks per kilometre of pipeline) for those respective areas.

Tools are developed that systematically allow an engineer to apply the derived correlations, including applying necessary corrections, to predict damage due to liquefaction induced lateral displacement and/or settlement. The tools also allow for an assessment of baseline damage due to shaking, as distinct from damage due to liquefaction.

This report has been developed with funding assistance from the Earthquake Commission (EQC) and the Quake Centre based at the University of Canterbury. It contributes to a body of guidance documentation being developed by a consortium of the Quake Centre, Water NZ and the Institute of Public Works Engineers Australasia (NZ) (IPWEA NZ). This guidance suite is called *Evidence-based Investment Decision-making for 3 Waters Pipe Networks* or simply the *Pipe Renewals Programme.*

List of Abbreviations

Abbreviation	Term
AAM	AAM Brisbane Ltd.
AC	Asbestos Cement
CBD	Central Business District
CCC	Christchurch City Council
CES	Canterbury Earthquake Sequence
CBD	Central Business District
CI	Cast Iron
CPT	Cone Penetration Testing
CRR	Cyclic Resistance Ratio
DEM	Digital Elevation Model
DI	Ductile Iron
EQC	Earthquake Commission
FS	Safety Factor
GMPGV	Geometric Mean Peak Ground Velocity
H_2	Thickness of liquefiable layer
IPWEA NZ	Institute of Public Works Engineers Australasia (NZ)
LiDAR	Light Detection and Ranging
LiDAR Zone	Geographical extent of LiDAR surveys in Christchurch before and after the 22 February 2011 earthquake
LINZ	Land Information New Zealand
LIQ Zone	Zones where liquefaction effects were observed in Christchurch during the 22 February 2011 earthquake
LPI	Liquefaction Potential Index
LSN	Liquefaction Severity Number
MPVC	Modified Polyvinyl Chloride
NOLIQ Zone	Zones where liquefaction effects were not observed in Christchurch during the 22 February 2011 earthquake
NZAM	New Zealand Aerial Mapping Ltd.

Abbreviation	Term
NZGD	New Zealand Geotechnical Database
PE	Polyethylene
PGA	Peak Ground Acceleration
PGD	Peak Ground Deformation
PGV	Peak Ground Velocity
PVC	Polyvinyl Chloride
RR	Repair Rate
RRAdd-Liq	Repair rate of additional damage caused by liquefaction effects
RRTGD	Repair rate caused by transient ground deformation effects
SAT Zone	Areas where satellite imagery is available
SCIRT	Stronger Christchurch Infrastructure Rebuild Team
SEGP	Polygon of Similar Expected Ground Performance
SV1D	Settlement Index
T+T	Tonkin + Taylor Ltd.
TGD	Transient Ground Deformation
TOT Zone	Geographical part of the wide-area model excluding the Port Hills area
UPVC	Unplasticised Polyvinyl Chloride
z	Depth below ground surface
ε_v	Calculated post-liquefaction volumetric reconsolidation strain

Table of Contents

1 Introduction 1

1.1 Purpose 1
1.2 Motivation 1
1.3 Previous work and limitations 2

2 Data sets 3

2.1 Pipe network data 4
2.2 Pipe repair data 11
2.3 GMPGV data 15
2.4 Areas of observed liquefaction effects 16
2.5 Ground surface subsidence data 16
2.6 Horizontal ground movement data 18
2.6.1 LiDAR derived horizontal displacements 18
2.6.2 Satellite imagery horizontal displacements 20
2.7 Liquefaction vulnerability parameter data 23

3 Data analysis 28

3.1 Relocation and de-clustering of the water system pipeline repair geospatial dataset 28
3.2 Geographical extents of analyses 29
3.3 Comparison of pipeline damage correlations with lateral displacements derived from different LiDAR and satellite imagery 30
3.4 Statistical analysis of pipeline damage 31
3.4.1 Comparison of RR in the NOLIQ zone and the LIQ zone 31
3.4.2 Statistical analysis with respect to GMPGV 33
3.4.3 Statistical analysis with respect to settlement 35
3.4.4 Statistical analysis with respect to lateral displacement 37
3.4.5 RR correlations of pipeline damage with the combined liquefaction-induced lateral displacement and settlement 38
3.4.6 Correlations between pipeline damage and LSN 40

4 Development of pipe repair rate functions 42

4.1 Methodology for assessing the additional pipeline damage caused by liquefaction-induced effects 42

4.1.1 Estimating the GMPGV breaks and RR_{TGD} 42

4.1.2 Adjusting the repair rate vs combined vertical and lateral displacements 43

4.1.3 Adjusting the repair rate vs LSN 44

5 Application 46

References 48

1 Introduction

1.1 Purpose

The purpose of this project is to develop assessment tools for pipeline damage based on correlations with liquefaction-induced ground movements and Cone Penetration Test (CPT)-based liquefaction metrics. Such correlations can be used by the engineering community for estimating pipeline damage following an earthquake and also for developing predictive models for pipeline damage in areas with liquefaction susceptible soils.

Pipeline damage correlations with liquefaction-induced lateral and vertical ground movements can be used to estimate pipeline repairs from the results of numerical simulations or hazard map assessments of liquefaction-induced ground deformation. They are also useful in estimating the damage within a pipeline network that has been subjected to liquefaction effects and identifying the areas where such damage is likely to have occurred following an earthquake. This approach is useful for triaging post-event damage assessment inspections.

Correlations between pipeline damage and liquefaction vulnerability index parameters derived from CPT results are useful in predicting the potential of pipeline damage from future earthquakes. Such correlations can be incorporated into probabilistic loss and network performance models. They could also be incorporated into the design process so new pipelines are designed with a performance objective of a repair rate less than a maximum accepted amount for the particular design level of earthquake shaking. This can feed into the *Evidence-based Investment Decision-making for 3 Waters Pipe Networks* guidance suite of documentation being develop by a consortium of the Quake Centre, Water NZ and IPWEA (NZ).

1.2 Motivation

This report builds on the methodology of previous geospatial correlations between pipeline damage and liquefaction-induced ground surface deformation (i.e., ground surface angular distortion and ground surface lateral strain) using LiDAR survey data (Bouziou, 2015; Bouziou and O'Rourke, 2015, Bouziou et al., 2015). While ground surface angular distortion and lateral strains are fundamental metrics directly related to pipeline deformation and damage, they are difficult to predict and cannot be easily or directly measured. Therefore, correlations between pipeline damage and liquefaction-induced settlement, and lateral displacement are developed in this work for easier and more straightforward application in practice. An additional advantage of the proposed methodology is that settlement and lateral displacement can be measured directly after an earthquake using remote sensing technologies such as LiDAR surveys and satellite imagery. Such liquefaction-induced

settlement and lateral displacement are positively correlated with ground surface angular distortion and lateral ground strain, respectively (i.e. larger vertical settlements and lateral movements result in an increased likelihood of higher angular distortions and lateral strains).

CPT measurements provide a direct assessment of liquefaction vulnerability and potential for ground deformation for various scenario earthquakes. They are also useful for predictive pipeline damage correlations. In contrast to ground movements, strains and angular distortion, they do not depend on the outcome of liquefaction, but on fundamental soil conditions that reflect the liquefaction vulnerability of a given site.

This report uses an extensive database of more than 25,000 CPT tests in the Christchurch area to investigate pipeline correlations with CPT-based liquefaction vulnerability index parameters.

1.3 Previous work and limitations

Previous work involved correlations of pipeline damage, expressed as pipeline repair rate (pipe repairs/km of pipeline length), with:

1. Peak Ground Velocity (PGV)
2. Ground surface angular distortion derived from LiDAR measurements (β)
3. Ground surface lateral strain derived from LiDAR measurements (ε)
4. Combined effects of ground surface angular distortion (β) and lateral ground stain (ε)

Ground surface angular distortion and lateral ground strain represent ground surface deformations which are the fundamental cause of pipeline damage. However, as discussed in Section 1.2, such parameters are difficult to predict and measure. Therefore, vertical settlement and lateral displacement can be used as proxies for ground surface angular distortion and lateral ground strain in pipeline damage correlations and such correlations provide for a more direct way of post-earthquake modelling for damage assessment screening.

2 Data sets

The spatial correlations of underground pipeline damage were developed based on the data sets pertaining to the 22 February 2011 earthquake. Accurate system-wide repair records are not available for the 4 September 2010 earthquake. At the time of 13 June 2011 earthquake, the pipeline system was affected substantially by widespread damage and repairs such that its physical condition differed appreciably from what would be encountered in a pre-earthquake water distribution system. Although the 4 September 2010 earthquake affected subsurface and pipeline conditions, its effects were confined to smaller areas. Moreover, the pipeline system had been repaired and restored to full functionality before the 22 February 2011 earthquake. Focusing on the effects of the 22 February 2011 earthquake, therefore, provides the best basis for developing correlations of underground pipeline damage with liquefaction-induced ground surface deformations and CPT-based liquefaction vulnerability index parameters.

The input data sets used in this project involve the geospatial data set of the water pipeline network in Christchurch (including pipe type, diameter and age), the water repair database provided by the Stronger Christchurch Infrastructure Rebuild Team (SCIRT) which includes information on spatially referenced continuous daily repair records for the re-establishment of services during the 2010-2011 Canterbury Earthquake Sequence (CES), the geospatial files of observed liquefaction effects for each earthquake event during the CES (van Ballegooy et al., 2015), the geospatial files of vertical and lateral LiDAR-based and satellite imagery based ground movements, and geospatial files of ground motion records from 40 stations in the Christchurch area.

Correlations between pipeline damage and CPT-based liquefaction index parameters were performed by collating liquefaction vulnerability indicators calculated from CPT data by van Ballegooy et al. (2015) and available in the New Zealand Geotechnical Database (NZGD) for the 4 September 2010 and 22 February 2011 earthquake events for areas of similar expected performance (Lacrosse et al., 2017).

The present study was performed using the most detailed and complete set of repair records pertaining to the water distribution system in Christchurch. However, the present study could be extended in the future to develop similar correlations for the storm water and wastewater networks provided that the respective repair datasets are similar in detail and completeness (or at least for smaller study areas).

2.1 Pipe network data

Approximately 1,700 km of water pipelines, which were geocoded by Christchurch City Council (CCC) and SCIRT, were used in this study to represent the pipeline network before the 22 February 2011 earthquake. The water supply network was fully reinstated after the 4 September 2010 earthquake prior to the 22 February 2011 earthquake. Hence, it is assumed that the water distribution system spatial dataset developed by SCIRT, and sourced originally by CCC, is also representative of the system before the occurrence of the 22 February 2011 earthquake. This dataset also provides the most complete picture of the system as of 4 September 2010.

The spatial dataset includes information about the type, diameter, material, length and year of installation for each individual pipe in the network (Cubrinovski et. al, 2014). The water distribution system included in this study includes water mains and trunk lines with diameters mainly between 75mm and 600mm, conveying the largest flows in the system. It does not include the smaller diameter submains and customer submains because reliable information about repairs for these pipes was not available at the time of this study. Moreover, water distribution networks in many other countries do not include submains, so that concentrating on the 75mm to 600mm diameter water mains in Christchurch provides results that are broadly applicable to water supply networks worldwide.

Water mains in Christchurch are typically laid in trenches 0.2-0.3 m wider than the pipe diameter, at relatively shallow depths (maximum depth 0.8m), and are located almost exclusively in the road corridors (Cubrinovski et al., 2014). The trenches are backfilled with native soils and are compacted to 95%, 90% and 70% of the material's maximum dry density (NZS 4402.4.1.1) for trafficked, pedestrian and landscape areas, respectively (Cubrinovski et al., 2014).

All of the Christchurch water is obtained from underground confined aquifers pumped from over 165 wells at more than 50 pumping stations, and then stored in 8 main reservoirs, 37 service reservoirs and 26 secondary pumping stations (Community and Public Health, 2016). The water is delivered into major trunk mains with diameters up to 600mm under pressure by electrically driven pumps. This network provides 100,000 cubic meters a day (100 million litres/day), totalling to about 36,525,000 cubic meters a year (36.5 billion litres/year) (Eidinger et al., 2012). The water system comprises of 7 pressure zones of which the Central Business District (CBD) is the largest. The mains generally comprise asbestos cement (AC) and cast iron (CI) followed by ductile iron (DI), polyvinyl chloride (PVC), modified polyvinyl chloride (MPVC) and unplasticised polyvinyl chloride (UPVC) pipe lines (Central City Assessment Report, 2016).

Table 2-1 summarises mains and trunk lines in the Christchurch water distribution system by material. The study presented in Sections 3 and 4 focuses on the three major pipe types in the Christchurch water supply system; AC, CI and PVC, whereas brief reference is made to other pipe types herein.

Table 2-1 Pipeline length by pipe material for water mains and trunk lines in the Christchurch water supply system.

Pipe Type	ID	Length (km)
Asbestos Cement	AC	867.24
Cast Iron	CI	194.37
Polyvinyl Chloride	PVC	212.69
Medium Density Polyvinyl Chloride	MPVC	149.72
Unplasticized Polyvinyl Chloride	UPVC	124.78
Concrete Lined Steel	CLS	52.02
Ductile Iron	DI	51.12
Concrete Lined Ductile Iron	CLDI	7.24
Steel	STEEL	36.55
Polyethylene 100	PE100	9.31
Polyethylene	PE	0.48
Medium Density Polyethylene 80	MDPE80	4.65
Medium Density Polyethylene 100	MDPE100	3.71
High Density Polyethylene	HDPE	2.42
Mortar Lined Ductile Iron	MLDI	2.54
Reinforced Concrete Rubber Ring	RCRR	0.20
Galvanised Iron	GALV	2.36

AC pipes were mainly introduced in the system in the 1960s (Figure 2-1a) and their production ceased in New Zealand in 1986 (Water New Zealand, 2017). They had been the primary pipe material installed in Christchurch in the decade following World War II, and, as shown in Table 2-1 they comprised the largest category of pipes in the Christchurch water supply system by the time the 22 February 2011 earthquake took place. AC pipes have diameters ranging from 100mm to 200mm (Figure 2-1b) and are typically connected with rubber ring coupling joints. The oldest AC pipes in the system were manufactured as a mixture of asbestos fibres, clay filler and cement, and have significant wall thickness, whereas the newer ones were a mixture of asbestos fibres and cement and have smaller wall thickness. Because of the decreased wall thickness, newer AC pipes are more deteriorated due to internal corrosion so, in some cases, they are weaker than the older AC pipes in the system.

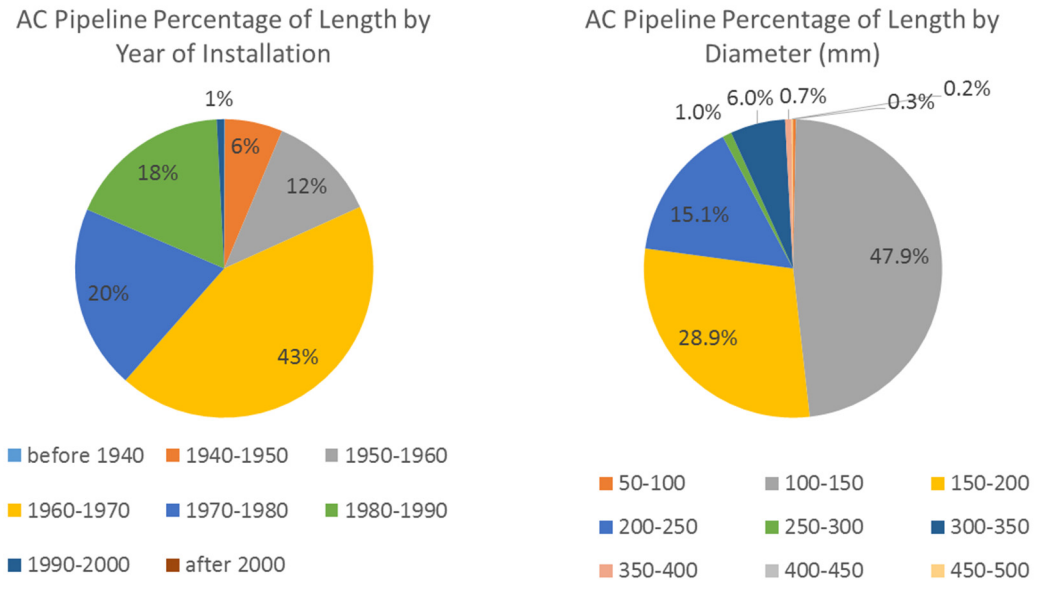

(a) **(b)**

Figure 2-1 Percentage of AC pipeline length by year of installation, and by diameter in the Christchurch water supply system.

CI pipes are among the oldest pipes in the Christchurch water supply system, dating to the 1890s (Figure 2-2a). Installation of these pipes stopped in the 1990s when PVC became the main pipe material for new installations in the water supply system (Figure 2-3a). The majority of CI pipes have diameters ranging from 100mm to 200mm (Figure 2-2b), and typically have rubber ring, lead wool or poured lead bell and spigot joints.

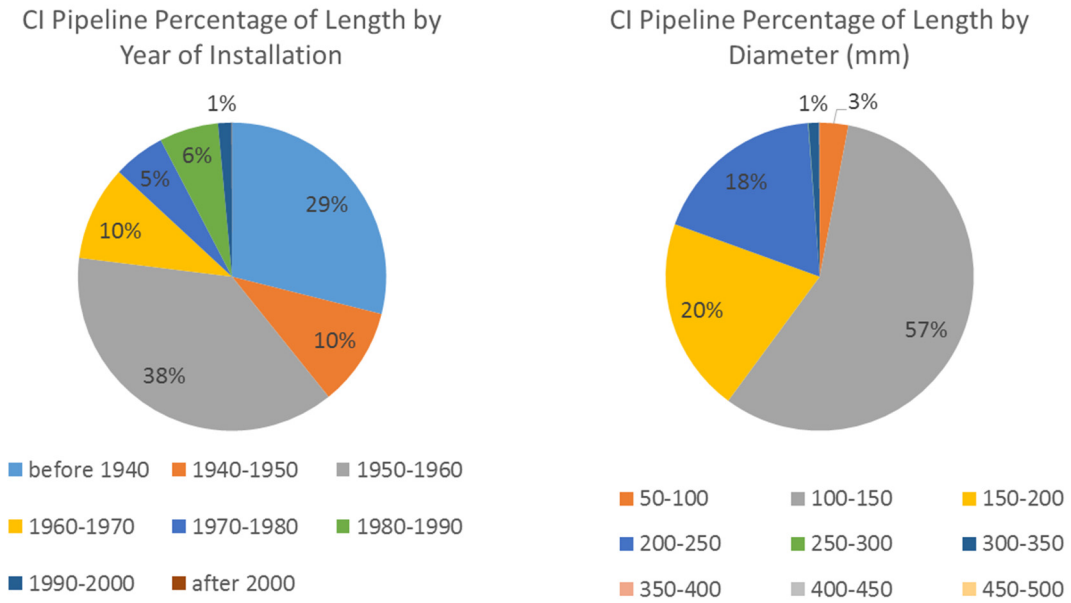

(a) **(b)**

Figure 2-2 Percentage of CI pipeline length by year of installation, and by diameter in the Christchurch water supply system.

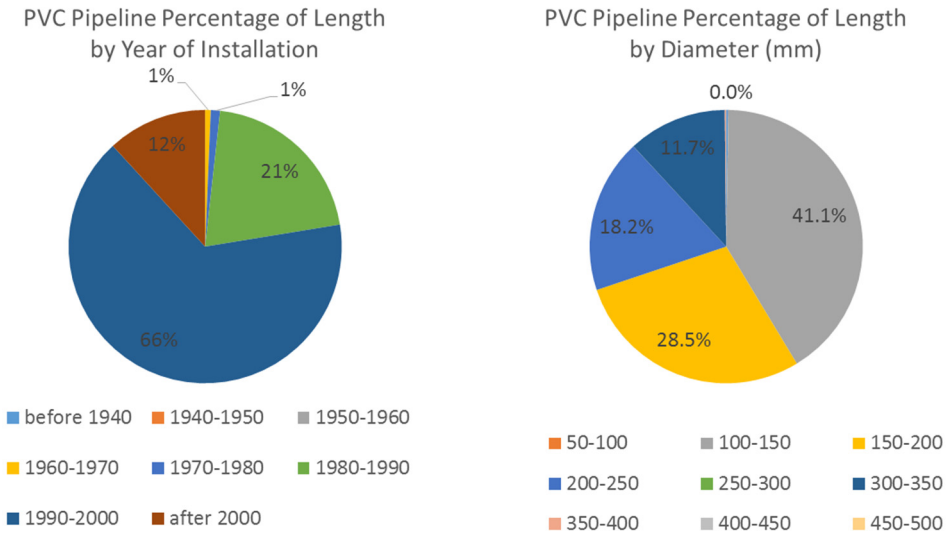

(a) **(b)**

Figure 2-3 Percentage of PVC pipeline length by year of installation, and by diameter in the Christchurch water supply system.

In recent years, three pipe materials have been used for water mains: ductile iron (DI), PVC (including modified PVC and unplasticised PVC) and polyethylene (PE), with a number of criteria being used in the selection of the pipe material (CCC, 2010). PE pipes are mostly used in the Christchurch gas pipe network, and are currently the predominant replacement pipe in the liquefiable east-central and eastern Christchurch (O'Callaghan, 2014). PVC pipes are installed in diameters ranging between 100mm and 200mm (Figure 2-3b) and have rubber ring joints with bell and spigot ends. PVC pipes were introduced in the Christchurch water supply system early in the 1960s and at that stage the quality of the PVC materials used was quite variable. The Christchurch water system also contains unplasticised polyvinyl chloride (UPVC) and modified polyvinyl chloride (MPVC) pipelines. Both UPVC and MPVC materials maintain the structure of PVC and have similar physical properties. In contrast to PVC, UPVC pipes do not contain plasticising polymers, and they are more resistant to deformations and chemical factors. MPVC is different from PVC by means of added modified agents that increase its ductility and stiffness.

The distribution of the water supply network in Christchurch by means of pipe type, diameter and age is summarised in Tables 2-1, 2-2 and 2-3 and spatially presented in Figures 2-4, 2-5 and 2-6 respectively, superimposed on the zone of observed liquefaction effects during the 22 February 2011 earthquake. As shown in Figure 2-4, AC pipes are evenly distributed in Christchurch, whereas CI and PVC pipes, and other pipe types, are mostly clustered in areas within the zone of observed liquefaction effects. Figure 2-2b indicates that the water supply system typically consists of small diameter pipelines (diameters less than 200mm), whereas pipelines with larger diameters are located in the southern outskirts of Christchurch and convey water from the reservoirs and pumping stations into the system.

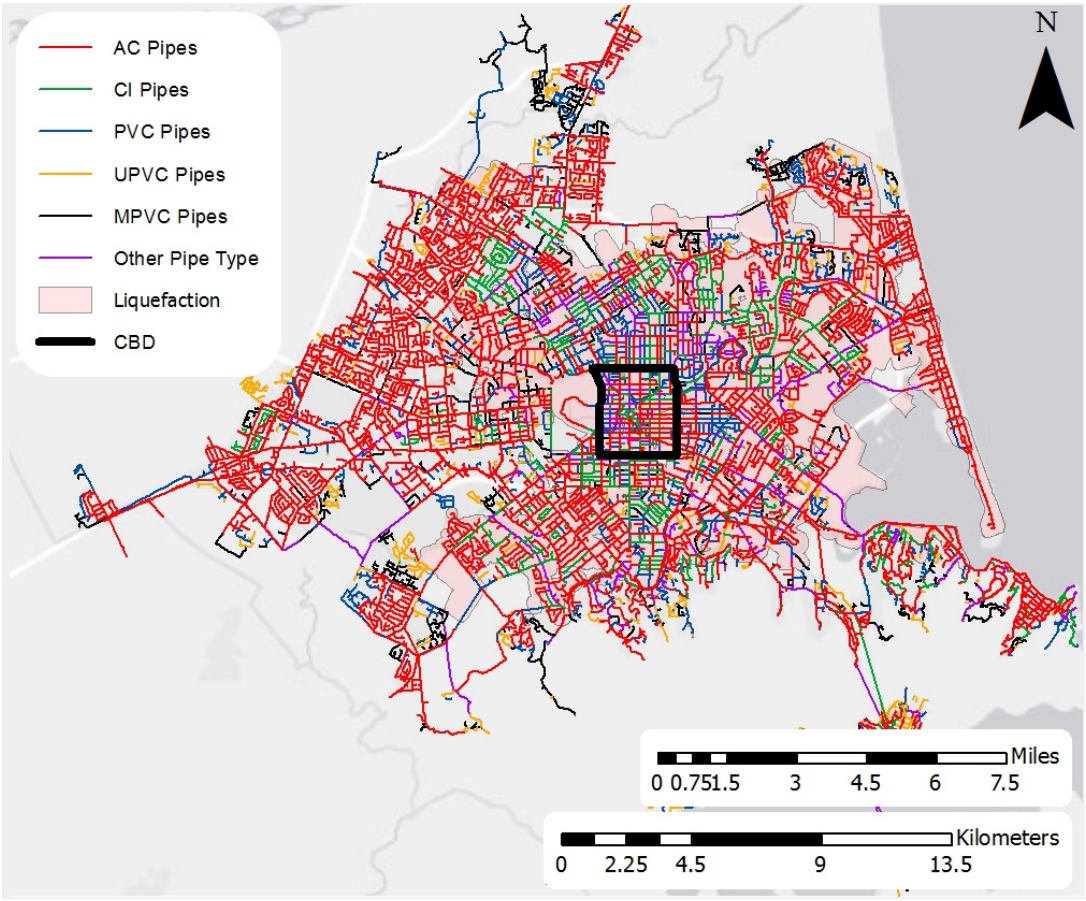

Figure 2-4 Potable water mains and trunk lines in Christchurch City according to pipe material at the time of the 22 February 2011 earthquake.

Table 2-2 Pipeline length by diameter for the AC, CI, PVC, UPVC and MPVC pipelines in the Christchurch water supply system.

Diameter (mm)	Pipe Length (km)				
	AC	CI	PVC	UPVC	MPVC
50-100	2.8	5.8	0.1	2.8	0.4
100-150	415.3	111.0	87.3	49.8	49.5
150-200	250.9	39.7	60.6	42.2	54.4
200-250	130.6	35.5	38.8	22.0	37.4
250-300	8.5	0.1	0.0	0.0	0
300-350	51.7	2.2	24.9	6.9	8.0
350-400	6.1	0.1	0.3	1.1	0
400-450	0	0	0.01	0	0
450-500	1.3	0	0.002	0	0
500-550	0	0	0.002	0	0
550-600	0	0	0.002	0	0

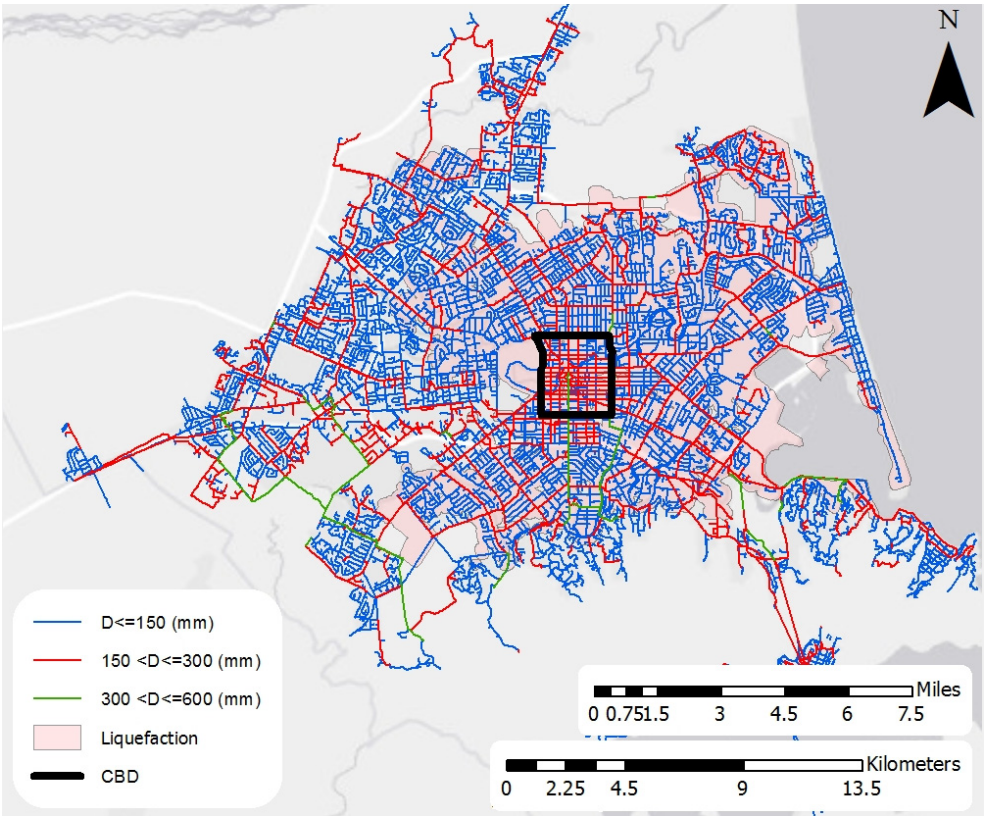

Figure 2-5 Potable water mains and trunk lines in Christchurch City according to pipe diameter at the time of the 22 February 2011 earthquake.

Table 2-3 Pipeline length by year of installation for the AC, CI, PVC, UPVC and MPVC pipelines in the Christchurch water supply system.

Year Laid	Pipe Length (km)				
	AC	CI	PVC	UPVC	MPVC
before 1940	0.6	56.1	0	0.04	0
1940-1950	54.2	20.0	0	0	0
1950-1960	103.0	73.2	0	0	0
1960-1970	374.5	19.3	1.4	0.002	0
1970-1980	172.6	10.6	2.3	0.3	0.0003
1980-1990	153.4	12.0	43.9	25.7	0.02
1990-2000	7.0	2.8	139.9	39.3	8.9
2000-2011	0.03	0.1	25.1	59.2	140.6

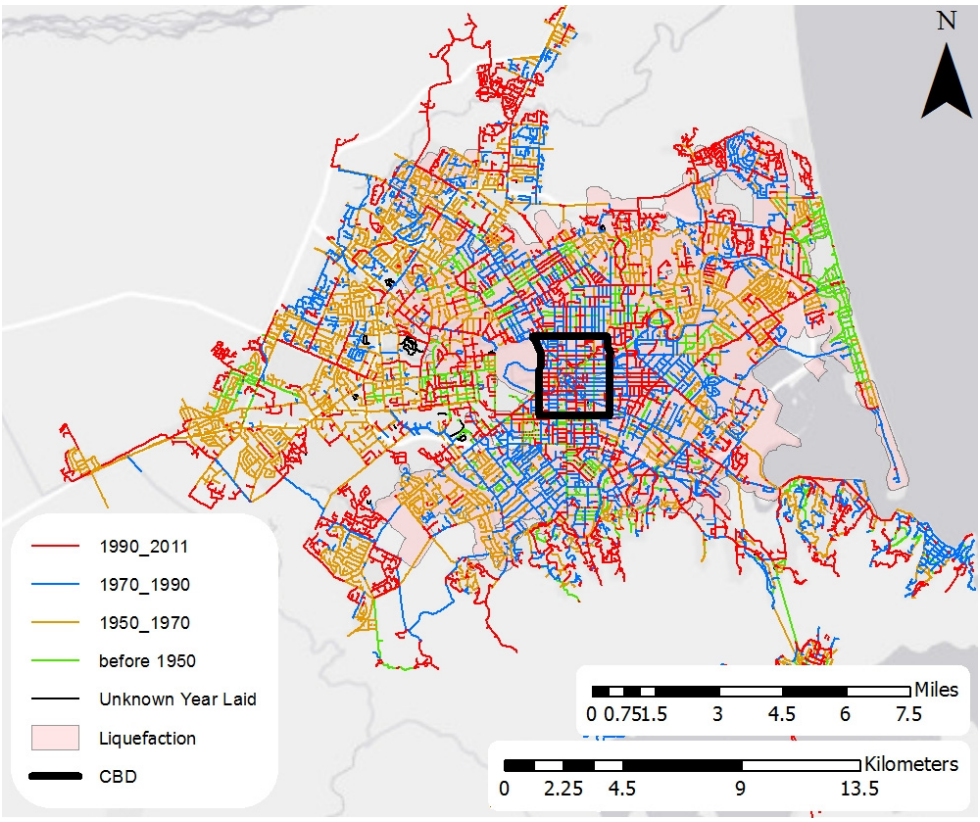

Figure 2-6 Potable water mains and trunk lines in Christchurch City according to pipe age at the time of the 22 February 2011 earthquake.

The water supply network in Christchurch is typically designed for an asset life of 100 years, which is also the minimum required design life of the pipes and fittings. Based on Table 2-1 and 2.3 the water supply network in Christchurch mainly consists of older AC pipes, a large proportion of which are close to the end of their design life. As shown in

Figure 2-6, the oldest pipes (i.e. AC and CI laid before 1970) are mainly located in western Christchurch, and several old pipes are also located in New Brighton, Dallington, Avondale and Aranui. The newest pipes are located mainly in the CBD and surrounding areas.

2.2 Pipe repair data

The water repair database provided by SCIRT includes information on continuous daily repair records for re-establishment of services between 23 February 2011 and 11 March 2013. The database includes repair on water mains and trunk lines with diameters mainly between 75 and 600mm, conveying the largest flows in the system. It does not include the smaller diameter submains and customer service laterals because the repairs for these pipes are not available. It is noted that the repairs were also affected by the subsequent 13 June 2011 and 23 December 2011 earthquakes and numerous aftershocks. SCIRT's geocoded repair dataset is used in the present study to reflect pipeline damage caused by the 22 February 2011 earthquake. Specifically, water distribution system repair records in the latest and more complete dataset, provided by SCIRT, and dating from 23 February to 15 April 2011 were related to the 22 February 2011 earthquake, according to the methodology developed by O'Rourke et al. (2014), and were used in this study.

Pipe repair data were supplied by infrastructure management company Citycare for each of the Christchurch potable water, wastewater and stormwater systems. During field surveys, damage to water supply pipes was found primarily from surface observations and pressure changes. Pipeline repairs were recorded by various contractors under emergency conditions, and the repair notes included in the database provide limited information about the type of repair, repair date, and length of pipe repaired. Nevertheless, the repair data are of great value in providing information about the repair location, type of pipe repaired, and field notes related to the repair.

Prior to using the water distribution network repair dataset in the present study, the GIS shapefile of repairs was reviewed, and it was observed that in several places the repair data have been recorded far from their actual location, and not always on top of their respective pipe segments, resulting in geospatial data with erroneously located (mislocated) repairs in the GIS shapefile. In several instances the same repair was recorded multiple times in the GIS shapefile. The process of relocating and de-clustering the water distribution repair dataset is described in detail in Section 3.1.

The geographical distribution of the recorded repairs in the Christchurch water supply system related to the 22 February 2011 earthquake are presented in Figure 2-7. The map shows that the majority of repairs are located within the zone of observed liquefaction effects, which also corresponds to the areas of visual observations of damage following the 22 February 2011 earthquake. Specifically, most of the repairs are located in the areas around the Avon River, especially in the CBD and the areas northeast of the CBD (i.e. Avonside, Dallington and Avondale) which were mostly affected by moderate to severe land damage due to liquefaction effects such as sand ejection and lateral spreading (van Ballegooy et al., 2014).

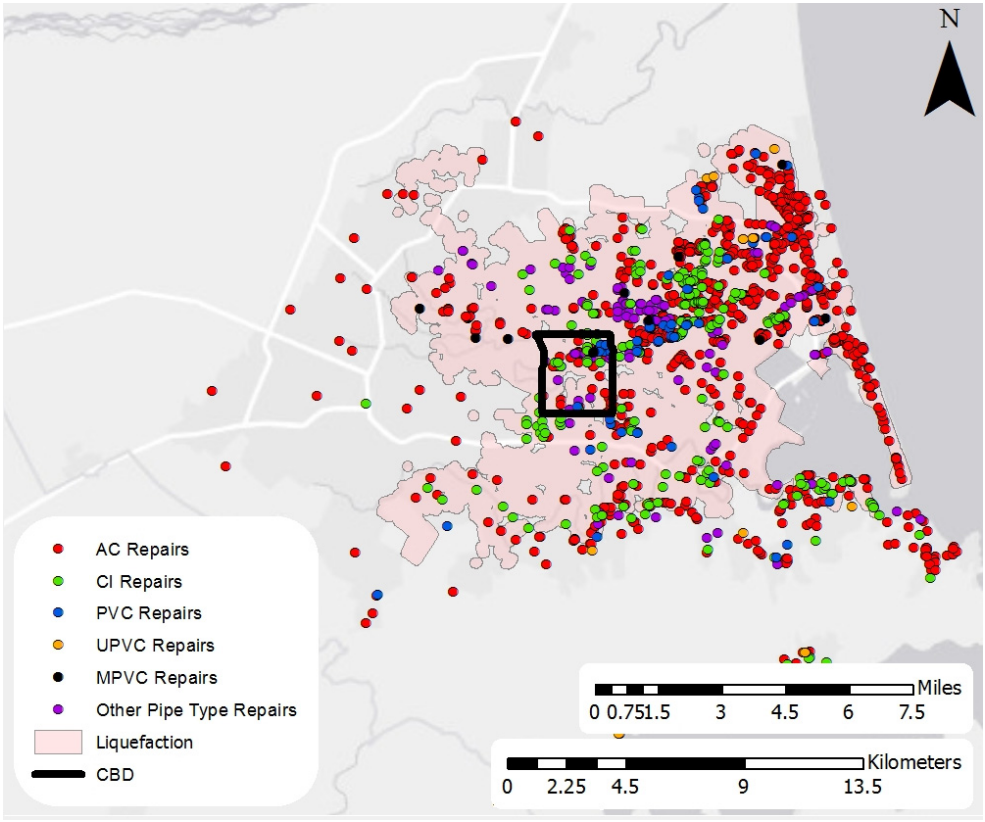

Figure 2-7 Geographic distribution of repairs on water mains and trunk lines in Christchurch City due to the 22 February 2011 earthquake.

As shown in Figure 2-7, AC pipelines were most severely affected by liquefaction, followed by CI pipes in the Christchurch water supply system.

Based on site observations after the 22 February 2011 earthquake, a significant percentage of pipe damage was related to joint and coupling failures (O'Callaghan, 2014). Observed modes of damage to AC pipes due to liquefaction effects include localised 45-degree compression fracture of rubber ring coupling joints and crushed spigot, leakage due to joint separation and pull-out of couplers, and localised shearing of spigot inside the bell. For CI pipelines, observed modes of damage are fracture of the bells of the joints, joint separation, localised pull-out of couplers, and displacement of screw gland and lead wool joints. PVC pipelines were damaged by means of joint separation, "telescoping" of joints, buckling, distortion and folding of pipe, for which there was limited leakage. Part of the PVC failure may also be attributed to poor quality PVC materials that were introduced in the water supply system in the 1960s.

The distribution of pipeline repairs by type, year of installation and pipe diameter are tabulated in Tables 2-4 and 2-5**Error! Reference source not found.Error! Reference source not found.**. As shown in Table 2-4**Error! Reference source not found.**, most of the damage occurred in old AC and CI pipes installed before 1980, and small diameter pipes (diameters between 100 and 200mm).

Table 2-4 Pipe repairs by year of installation for AC, CI, PVC, UPVC and MPVC pipelines in the Christchurch water supply system.

Year Laid	Pipe Repairs				
	AC	CI	PVC	UPVC	MPVC
before 1940	0	76	0	0	0
1940-1950	136	19	0	0	0
1950-1960	219	109	0	0	0
1960-1970	279	21	0	0	0
1970-1980	208	16	2	0	0
1980-1990	163	10	16	7	0
1990-2000	18	3	46	8	0
2000-2011	0	0	4	3	13

Table 2-5 Pipe repairs by diameter for AC, CI, PVC, UPVC and MPVC pipelines in the Christchurch water supply system.

Diameter (mm)	Pipe Repairs				
	AC	CI	PVC	UPVC	MPVC
50-100	1	9	0	0	0
100-150	670	145	49	12	7
150-200	202	55	11	1	4
200-250	117	44	5	3	2
250-300	2	0	0	0	0
300-350	32	2	3	2	0
350-400	0	0	0	0	0
400-450	0	0	0	0	0
450-500	0	0	0	0	0
500-550	0	0	0	0	4
550-600	0	0	0	0	0

To compare the results of pipeline damage due to the 22 February 2011 earthquake for different types of pipe, age and diameters, the repair rate (RR), expressed as repairs per kilometre, was calculated from the information in Table 2-4**Error! Reference source not found.** to **Error! Reference source not found.**2-5 and presented in Table 2-6 and Table 2-7. A green-to-red colour scale is used for each cell, indicating the range from the lowest to the highest values of RR, respectively. The highest RRs are sustained by AC and CI pipelines with roughly equal rates of repair. Older pipes and pipes with smaller diameters sustained relatively greater amounts of damage. PVC pipes, and especially UPVC and MPVC performed significantly better compared to AC and CI pipes. RR values corresponding to pipeline lengths less than 5km are not included in Tables 2-6 and 2-7.

Table 2-6 Pipe repair rate by year of installation for AC, CI, PVC, UPVC and MPVC pipelines in the Christchurch water supply system.

Year Laid	Repair Rate (Repairs/km)				
	AC	CI	PVC	UPVC	MPVC
< 1940	-	1.4	-	-	-
1940-1950	2.5	0.9	-	-	-
1950-1960	2.1	1.5	-	-	-
1960-1970	0.7	1.1	-	-	-
1970-1980	1.2	1.5	-	-	-
1980-1990	1.1	0.8	0.4	0.3	-
1990-2000	2.6	-	0.3	0.2	0.0
2000-2011	-	-	0.2	0.1	0.1
All <1940 - 2011	**1.2**	**1.3**	**0.3**	**0.1**	**0.1**

Table 2-7 Pipe repair rate by diameter for AC, CI, PVC, UPVC and MPVC pipelines in the Christchurch water supply system.

Diameter (mm)	Repair Rate (Repair/km)				
	AC	CI	PVC	UPVC	MPVC
50-100	-	1.5	-	-	-
100-150	1.6	1.3	0.6	0.2	0.1
150-200	0.8	1.4	0.2	0.0	0.1
200-250	0.9	1.2	0.1	0.1	0.1
250-300	0.2	-	-	-	-
300-350	0.6	-	0.1	0.3	0.0
350-400	0.0	-	-	-	-
400-450	-	-	-	-	-
450-500	-	-	-	-	-
500-550	-	-	-	-	-
550-600	-	-	-	-	-
All 50 - 600	**1.2**	**1.3**	**0.3**	**0.1**	**0.1**

2.3 GMPGV data

Ground motion records from 40 stations in the Christchurch area were selected to derive the distribution of peak ground velocity related to the 22 February 2011 earthquake. The selected records were fully processed by GNS Science (2013) to provide acceleration, velocity and displacement time histories and response spectra using a filtering process (Bouziou, 2015). The geometric mean peak ground velocity (GMPGV) was calculated for each station as the mean of the natural logs of the two maximum values of horizontal PGV recorded at the station, with the methodology described by Bouziou (2015), and its distribution in the Christchurch area is presented in Figure 2-8 superimposed by the zone of observed liquefaction effects.

The response of the water distribution system in Christchurch outside the zone of observed liquefaction effects was evaluated through pipeline RR correlations with GMPGV.

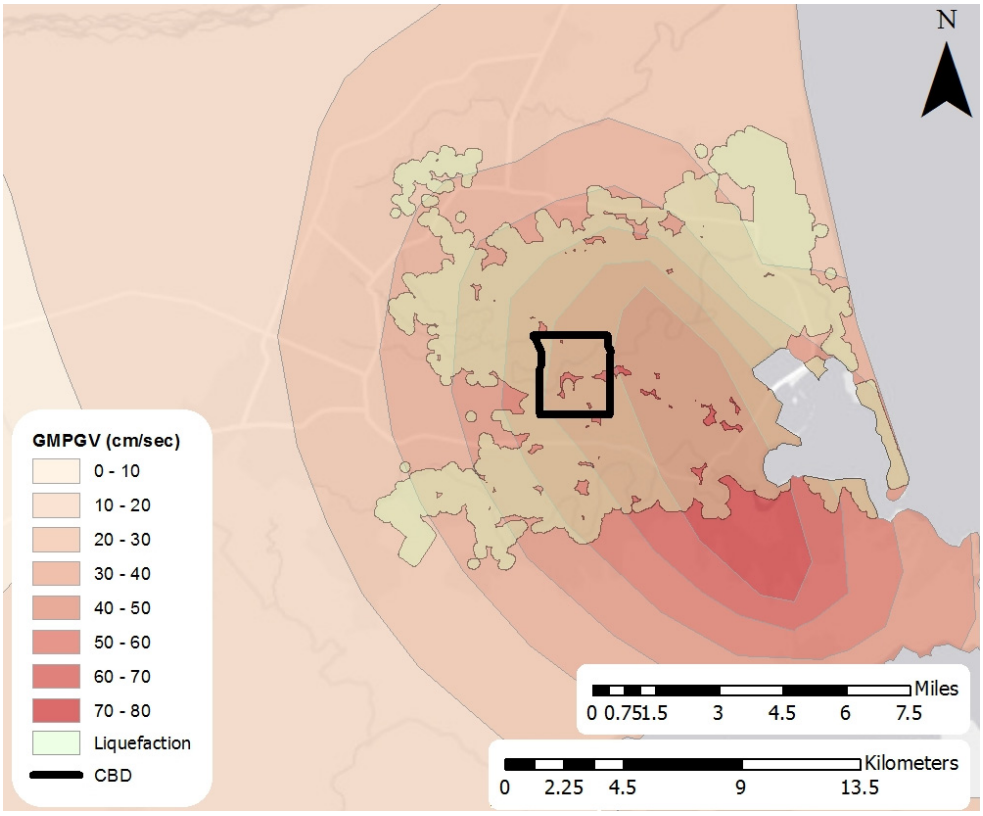

Figure 2-8 Map of GMPGV model developed by Bouziou (2015) and areas of observed liquefaction effects.

2.4 Areas of observed liquefaction effects

Liquefaction related land damage mapping of residential properties was carried out by teams of geotechnical engineers and engineering geologists immediately after the September 2010, February 2011 and June 2011 earthquakes to assess the extent and severity of the surface effects of liquefaction. In addition to site observations, aerial photography after each of the four main earthquakes was undertaken to identify areas where liquefaction ejecta occurred, part of which may have been cleaned up by the time the ground teams arrived (Tonkin + Taylor, 2015). Observed liquefaction effects include sand ejecta, as well as ground cracking, lateral spreading and differential surface settlement.

A GIS shapefile, combining the ground and aerial observations showing the areas of observed liquefaction effects for the 22 February 2011 earthquake, was used in this study. Areas outside this zone may also have had soil layers that liquefied but without surface manifestations of liquefaction. Therefore, the defined areas of observed liquefaction provide only an estimate of the extent of liquefaction in Christchurch after the 22 February 2011 earthquake.

As explained by Bouziou (2015), the areas of observed liquefaction effects were expanded to account for a zone of influence at the perimeter of the liquefaction areas that affects underground pipelines. The zone of influence of underground pipeline damage was taken as 125m, which is approximately one-half a typical street length in a residential neighbourhood and is consistent with the distance that significant pull-out forces can be transmitted longitudinally along underground pipelines (O'Rourke and Liu, 1999). These areas are described in this study as the zone of observed liquefaction effects (LIQ Zone) and are illustrated in Figure 2-8

2.5 Ground surface subsidence data

Airborne LiDAR surveys were collected before and after each of the main earthquake events in the CES by AAM Brisbane Pty. (AAM) and New Zealand Aerial Mapping Ltd. (NZAM) to assess ground surface elevation changes attributable to each main earthquake event. Pairs of these data were used by Tonkin + Taylor Ltd. (T+T) to determine vertical ground surface movements developed during the CES. The LiDAR elevation point clouds were used to develop bare earth digital elevation models (DEMs) at 5m spacing by averaging the ground-return elevations within 5m x 5m cells. These DEMs were further corrected for tectonic movement using a dislocation model of the vertical tectonic movements during the 22 February 2011 earthquake by GNS Science (2013). Tectonic movements were subtracted from the set of vertical ground surface LiDAR elevation changes to obtain elevation changes caused by liquefaction effects.

Figure 2-9 illustrates the distribution of the calculated liquefaction-related ground surface elevation change in the Christchurch area that was derived from LiDAR surveys before and after the 22 February 2011 earthquake.

The accuracy and limitations of the LiDAR surveys are mainly governed by the measurement error in the LiDAR points, localised error due to interpolation in areas with low density of points reflecting the ground surface (i.e. ground classified points), and spatial resolution of the DEM and its accuracy in representing the ground surface elevation (Tonkin + Taylor, 2015). The vertical LiDAR point clouds and the bare earth DEMs measured before and after each earthquake were calibrated against field survey data supplied by CCC, Land Information New Zealand (LINZ) and Environment Canterbury from surveys of their benchmark networks (Canterbury Geotechnical Database, 2012). Overall, the LiDAR point clouds are shown to have mean and median error of less than 50mm, suggesting reasonable accuracy as a whole (Tonkin + Taylor, 2015).

The calculated ground surface elevation change in Christchurch caused by the 22 February 2011 earthquake and derived from LiDAR surveys, with the vertical tectonic movements removed, is presented in
Figure 2-9. Most of the elevation changes in Christchurch involve subsidence of the ground surface which is concentrated primarily in the areas surrounding the Avon River.

There is a distinct area of lower subsidence which runs parallel to the September 2010 flight path (Tonkin + Taylor, 2015) suggesting banding error in the LiDAR data set of September 2010. Based on the comparative analysis of the error bands in the DEM difference maps presented in Tonkin + Taylor (2015), the September 2010 DEM elevations as an average are approximately 100mm lower in this identified zone than the actual ground surface (shown in Figure 2-9).

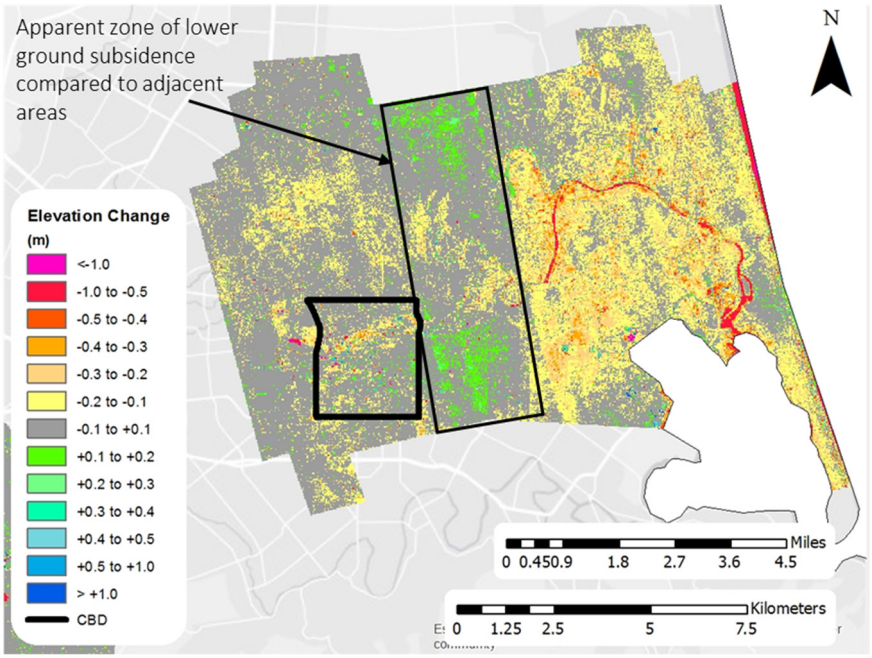

Figure 2-9 Map of the calculated liquefaction-related ground surface elevation change derived from LiDAR surveys before and after the 22 February 2011 earthquake.

2.6 Horizontal ground movement data

2.6.1 LiDAR derived horizontal displacements

Lateral movements were also derived from the Airborne LiDAR surveys before and after each main earthquake event. Sub-pixel correlation using 64x64 pixel windows was developed by Imagin'Labs Corporation, Pasadena, CA, and California Institute of Technology (Beavan et al., 2012) to derive horizontal displacement information from the gridded LiDAR. A significant part of instrument artefacts, such as laser wavelength jitter contained in the LiDAR data, was removed by eliminating the horizontal and vertical stripes in the collected images (i.e. destripping). Poor correlation values, as well as correlation values presenting unreasonable displacements, were discarded to improve the quality of the data sets. The resulting LiDAR sets were finally filtered using a modified version of the Non-Local Mean Filter to reduce noise (Beavan et al., 2012). The filtering process, however, incurred loss of spatial resolution. Therefore, a comparative study was performed to determine the most appropriate dataset for LiDAR displacement (i.e. filtered or unfiltered) for use in spatial correlations with pipeline damage. The LiDAR displacement maps were originally developed at 4m and 8m spacings and were averaged to provide lateral movements at 56m spacing. LiDAR lateral displacements on 4m spacing grids are consistent with typical pipeline lengths of 4-6m and provide higher resolution of the strain fields affecting pipelines (Bouziou, 2015). Accordingly, they are used in the present study to correlate pipeline damage with LiDAR lateral displacements.

The AAM LiDAR horizontal accuracy, compared to land survey measurements supplied by CCC, LINZ and Environment Canterbury, is 40 to 55cm (Beavan et al., 2012). Hence, 2-D displacements greater than approximately 40cm can be reliably detected over large parts of each image, except for areas of significant noise. Overall, the LiDAR dataset pertaining to the 22 February 2011 earthquake appears to contain the most reliable measurements of lateral LiDAR movement during the CES (Tonkin + Taylor, 2015).

These liquefaction-related ground surface lateral displacements were calculated by removing the tectonic component of lateral ground surface movement from the collected LiDAR measurements using a dislocation model of the lateral tectonic movements during the 22 February 2011 earthquake proposed by GNS Science (2013).

Lateral spreading due to liquefaction caused permanent lateral displacements of more than 2m in the neighbourhoods along the Avon River to the east of the CBD (Cubrinovski et al. 2011). The highest levels of lateral displacement in the unfiltered and the filtered LiDAR data sets are concentrated in the areas surrounding the Avon River, whereas there are several other random areas shown in the unfiltered LiDAR data set with very high levels of lateral displacement. However, the latter are affected by the noise contained in the unfiltered LiDAR data, which is filtered out and smoothed in Figure 2-11.

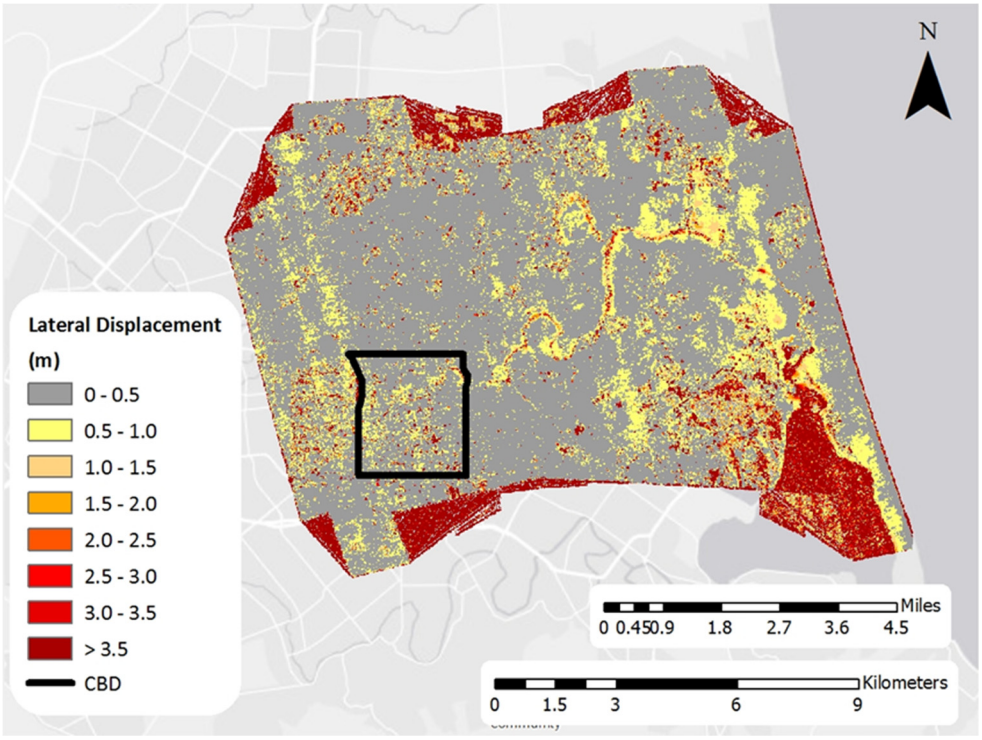

Figure 2-10 Map of the calculated liquefaction-related ground surface lateral displacements derived from the LiDAR surveys (without filtering applied) before and after the 22 February 2011 earthquake.

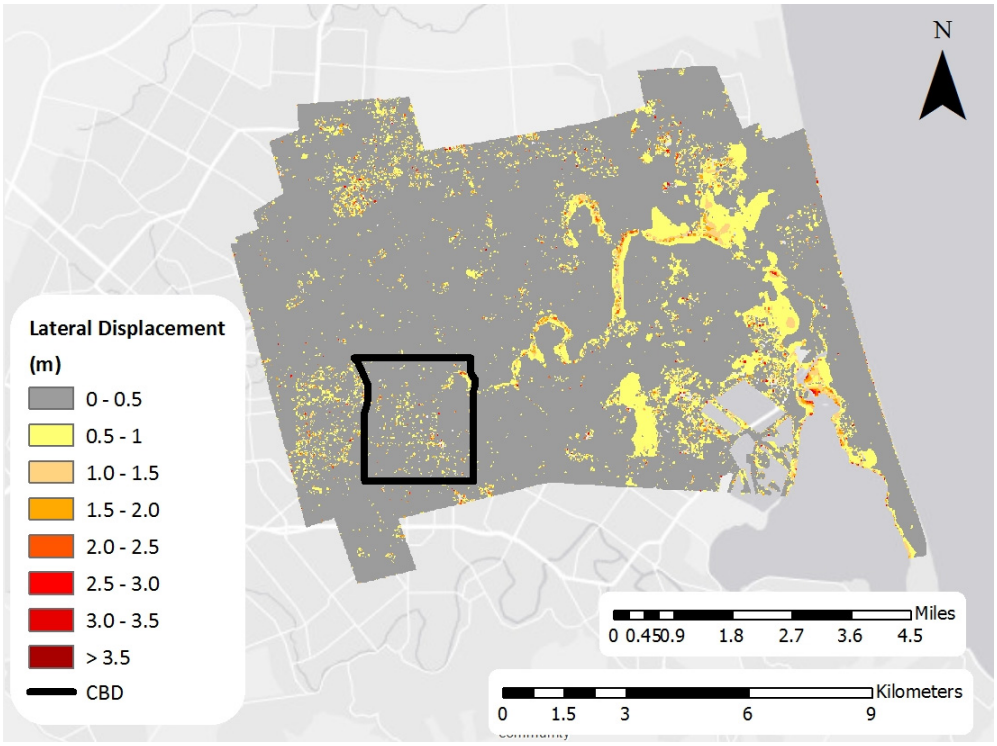

Figure 2-11 Map of the calculated liquefaction-related ground surface lateral displacements derived from the LiDAR surveys (with filtering applied) before and after the 22 February 2011 earthquake.

2.6.2 Satellite imagery horizontal displacements

In addition to airborne LiDAR surveys, pre- and post-earthquake images from the February 22, 2011 Christchurch earthquake were selected based on their similar acquisition angles and 0.5m pixel resolution. These panchromatic satellite image pairs were collected by the WorldView-1 (pre-event) and GeoEye-1 (post-event) satellites (Martin, 2014). The two images were subsequently orthorectified and subjected to co-registration and optical image correlation as described by Martin (2014). A precision displacement threshold of 0.3m was established that represents the potential variation between the measured and actual displacement, as well as the smallest displacement that can be confidently distinguished from zero. The area of analysis using the satellite imagery data was focused on the neighbourhoods along the Avon River to the east of the CBD, as shown in Figure 2-11.

Figure 2-12 illustrates the distribution of the calculated liquefaction-related lateral displacements derived from satellite imagery. Similar to Figure 2-10 and 2-11, the highest levels of lateral displacement are concentrated along the Avon River and most of the lateral displacements are located within 300m from the river banks, whereas high levels of lateral displacement extend beyond 500m in Avondale and New Brighton. A significant amount of displacement is captured in New Brighton by filtered and unfiltered LiDAR, and satellite imagery, as shown in Figures 2-10 and 2-11. The largest displacements are on the order of 2m or more, as captured by filtered LiDAR data and satellite imagery, whereas for unfiltered LiDAR data these displacements exceed 3m.

Figure 2-12 Map of the calculated liquefaction-related ground surface lateral displacements derived from the satellite imagery before and after the 22 February 2011 earthquake.

Figure 2-13 compares the liquefaction-related lateral displacements derived from unfiltered and filtered LiDAR, and satellite imagery, in the areas where satellite imagery is available (hereafter referred to as the SAT Zone). Overall, filtered LiDAR lateral displacements agree well with the satellite imagery results, even in the areas further from the river. Unfiltered LiDAR, however, are associated with higher levels of lateral displacement for the same areas and seem to have significant levels of noise. Given the noise in the unfiltered LiDAR data and the fact that satellite imagery restrains subsequent analyses to a much smaller geographic area than the LiDAR coverage, the filtered LiDAR lateral displacements were selected and used in this work to investigate correlations between pipeline damage and liquefaction-induced lateral movements. A comparative study of RR correlations with unfiltered and filtered LiDAR displacements as well as satellite imagery is presented in Section 3.3.

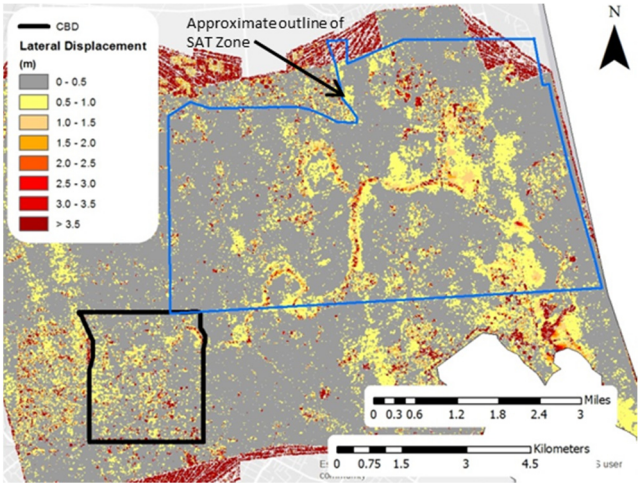

(a)

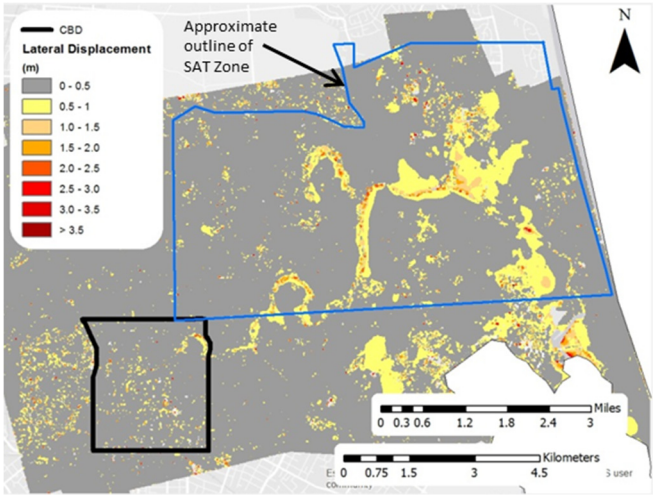

(b)

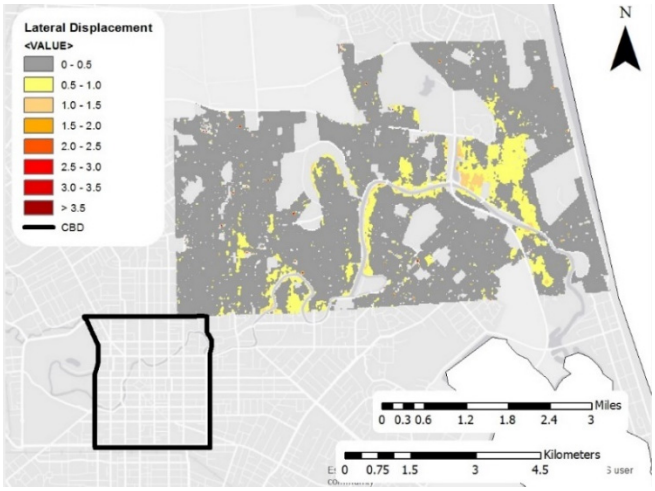

(c)

Figure 2-13 Comparison of liquefaction-related lateral displacements derived from: a) unfiltered LiDAR, b) filtered LiDAR and c) satellite imagery, in the areas covered by satellite imagery (SAT Zone).

2.7 Liquefaction vulnerability parameter data

Following the CES an extensive geotechnical investigation program was undertaken to inform the repair and rebuild. This included more than 25,000 CPT. CPT-based liquefaction vulnerability parameters were developed, and their efficacy evaluated for the purpose of estimating the liquefaction damage potential for foundation design purposes.

The liquefaction vulnerability parameters that were evaluated included the Liquefaction Potential Index (LPI), calculated settlement index (S_{V1D}) and the Liquefaction Severity Number (LSN). The development, observations and calculations related to the application LSN in Christchurch are described in detail in van Ballegooy et al., (2014 and 2015) and Tonkin + Taylor (2015). LSN is defined as:

$$LSN = 1000 \int \frac{\varepsilon_v}{z} dv \quad \text{(Eq. 2-1)}$$

where ε_v is the calculated post-liquefaction volumetric reconsolidation strain entered as a decimal and z is the depth below the ground surface in metres. LSN is calculated as the summation of the post-liquefaction volumetric reconsolidation strains calculated for each soil layer divided by the depth to the midpoint of that layer. The value of LSN is theoretically between 0 (representing no liquefaction vulnerability) to a very large number (representing extreme liquefaction vulnerability).

LPI (Iwasaki et al., 1982) is defined as:

$$LPI = \int_0^{20} F_1 W(z) dz \quad \text{(Eq. 2-2)}$$

where $W(z) = 10 – 0.5z$, $F_1 = 1 – FS$ for $FS < 1.0$, $F_1 = 1$ for $FS \geq 1.0$, and z is the depth below the ground surface in metres.

The calculated settlement indicator (S_{V1D}) is based on published methods to estimate volumetric shear strains, and these strains are integrated to calculate ground settlement.

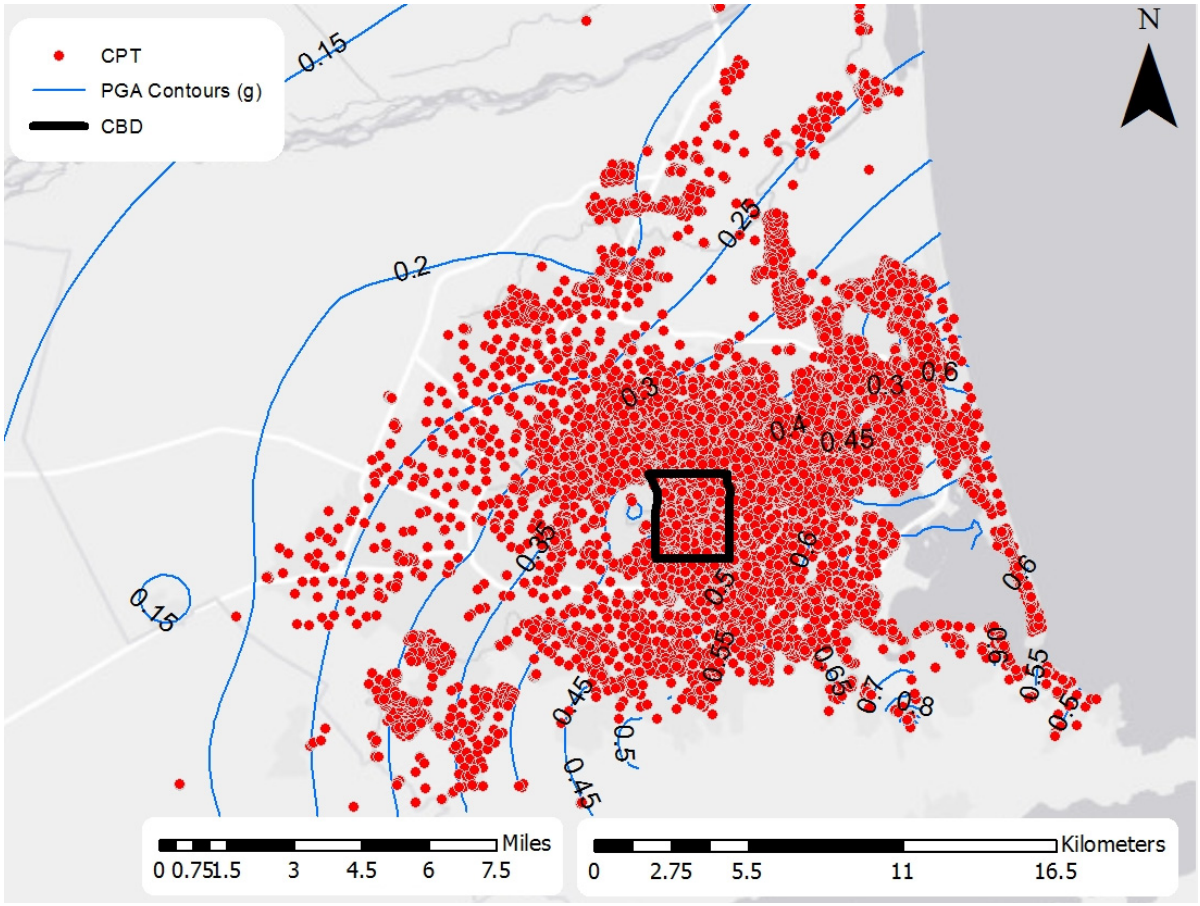

Figure 2-14 Map of CPT locations and PGA contours by Bradley and Hughes (2013) for the 22 February 2011 earthquake.

After consideration of other liquefaction-triggering methodologies, the safety factor FS and the thickness of the liquefiable layer (H_2) at each CPT location was determined by Tonkin + Taylor (2013) using the Idriss and Boulanger (2008) liquefaction triggering evaluation procedure. The assumed PGA at each of the CPT locations was based on the PGA contour models developed by Bradley and Hughes (2013), which are illustrated in Figure 2-14. Groundwater levels at the time of each earthquake were estimated using a regional groundwater model developed by Tonkin + Taylor (2013).

Based on a comparative study of these parameters by Tonkin & Taylor (2013), it was concluded that LSN provides the best correlations with land damage observations in Canterbury, and thus is the most suitable tool for predicting future land damage performance in Canterbury.

The LSN parameter was used to develop a regional liquefaction vulnerability model to predict liquefaction damage for different earthquake scenarios. This model was developed for the Earthquake Commission (EQC) as part of the Minerva loss model (in press). The regional liquefaction model has been used in the present study as the primary CPT-based liquefaction vulnerability index parameter to be correlated with pipeline damage.

To develop the liquefaction vulnerability model, the entire area was divided into polygons of similar expected ground performance. The following datasets were considered when mapping these polygons:

- Geological maps;
- Geomorphology maps;
- Location of waterways;
- Ground surface elevation;
- Depth to groundwater models; and
- Geotechnical data (mainly CPT and borehole logs).

The polygons were based initially on published geology and geomorphology maps (GNS, 2016) and then divided so each polygon had similar elevation and similar depth to groundwater conditions. The elevation models were derived from LiDAR datasets. The median depth to groundwater surface for the Christchurch area (van Ballegooy et al., 2014) was utilised.

The polygons were subdivided further when the ground conditions (as indicated by geotechnical investigation data) were sufficiently different in one part of a polygon compared to the rest of the polygon. The amount of data available for each polygon ultimately determined how coarse or finely detailed the polygons of similar expected ground performance are (i.e. the more data available, the higher the resolution and the smaller the polygons).

LSN values were calculated at each CPT location based on the Boulanger and Idriss (2014) liquefaction triggering method using the 50th percentile probability of liquefaction (P_L) cyclic resistance ratio (CRR) curve. LSN values were subsequently grouped together for each polygon of similar expected ground performance (SEGP). LSN distributions vs earthquake shaking, expressed as Peak Ground Acceleration (PGA), were developed for each SEGP. From these LSN distributions, the 50th and 75th percentile values of LSN in each SEGP were selected in the present study to investigate the effectiveness of LSN application in pipeline damage correlations.

The distribution of the 50th and 75th percentile values of LSN within each SEGP for the 22 February 2011 earthquake are presented in Figures 2-15 and 2-16. The analysis of LSN using the SEGP methodology was performed throughout the Christchurch area. In addition, the effectiveness of CPT-based index parameters for liquefaction vulnerability in predicting pipeline damage was investigated with this wide-area LSN model. The Port Hills area was excluded from the analyses because pipeline damage during the 22 February 2011 earthquake in this area was attributed to non-liquefaction-related permanent ground surface deformations (PGD) and ground failure mechanisms, such as landslides and rock falls (Bouziou, 2015).

The remaining geographical part of the wide-area model was used as one of the geographical extents in subsequent analyses and correlations and is hereafter referred to as the TOT Zone.

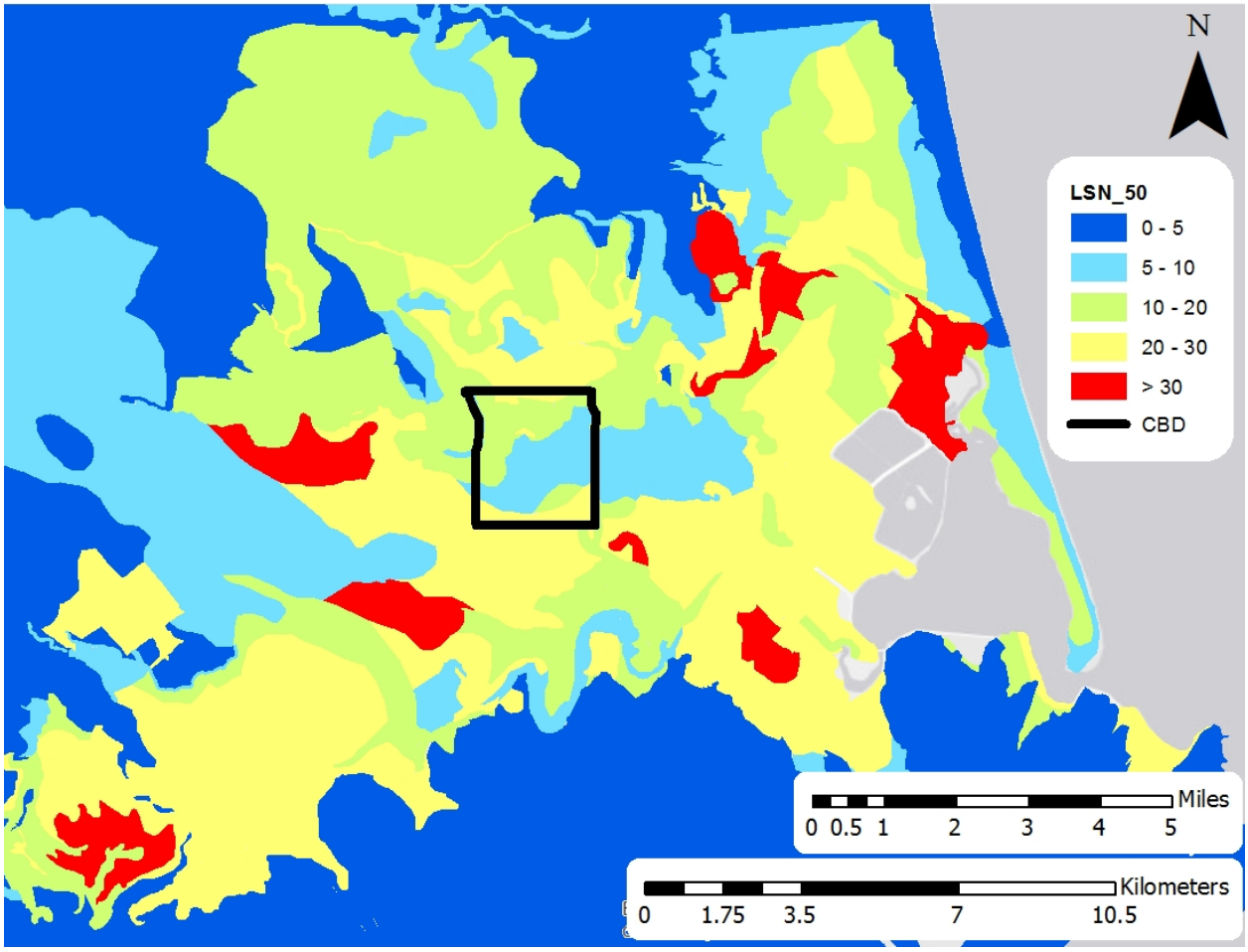

Figure 2-15 Map of 50th percentile LSN values by area of similar expected ground performance for the February 2011 earthquake.

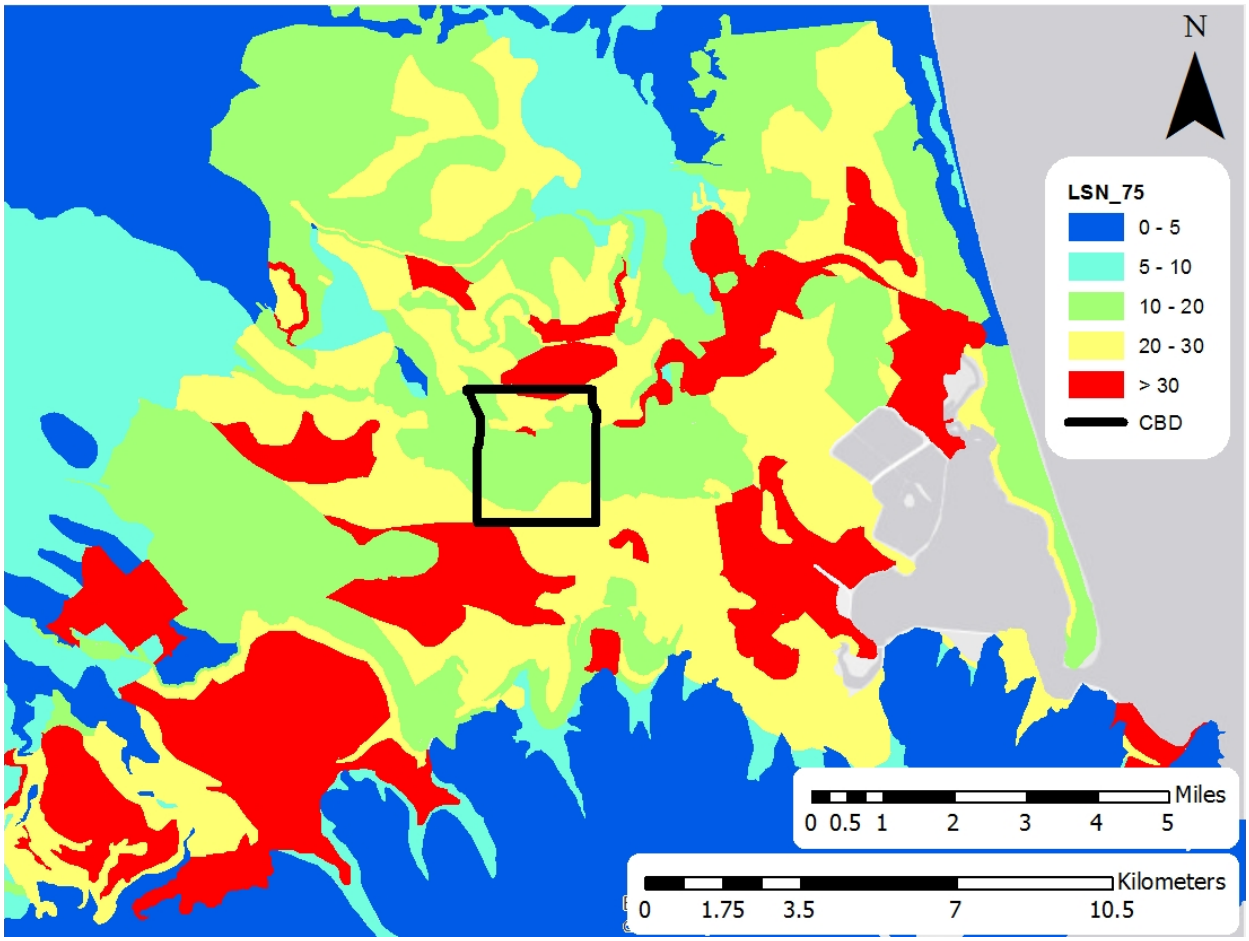

Figure 2-16 Map of 75th percentile LSN values by area of similar expected ground performance for the February 2011 earthquake.

3 Data analysis

3.1 Relocation and de-clustering of the water system pipeline repair geospatial dataset

As briefly described in Section 0, the water distribution network repairs were reviewed and corrected for misplacement and clustering of pipe repair records. Several repair data were georeferenced far from their actual locations in the field. Repair data were not always linked to their respective pipe segments, resulting in mislocated geospatial repair data that were not located on the appropriate damaged pipelines. Moreover, several repairs in the GIS shapefile were clustered in several locations, indicating that the same repair was recorded multiple times. Figure 3-1(a) and Figure 3-1(b) illustrate two characteristic examples of repair relocation and de-clustering, respectively, for the AC repair dataset.

The actual location of a repair was determined by using the unique pipe identifier to relocate each repair to its respective damaged pipe segment. During de-clustering, repairs located within a 2m radius from each other were de-clustered by merging them into one single repair data point.

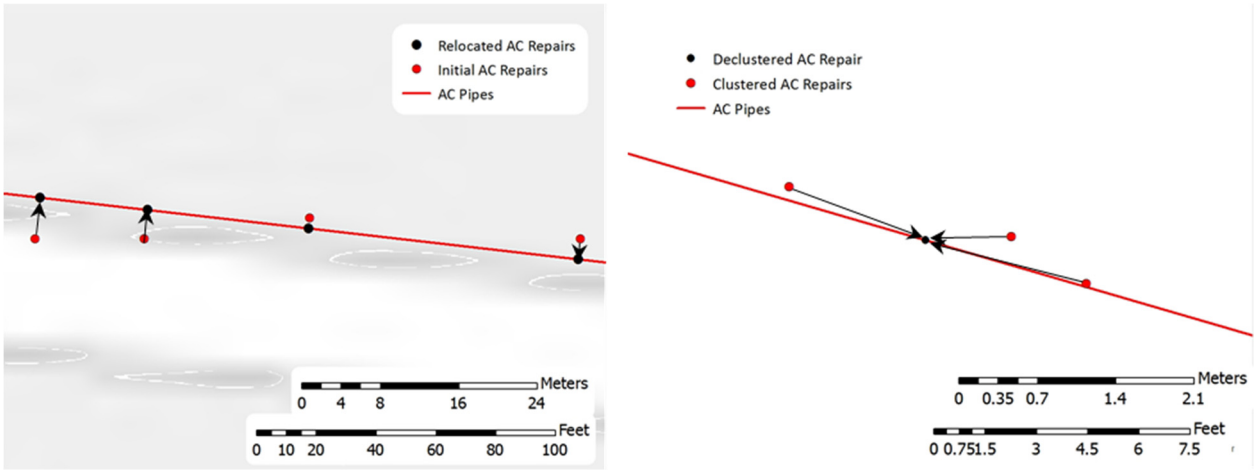

(a) **(b)**

Figure 3-1 Examples of: a) repair inaccurate location in the geospatial data set, b) repair clustering and inaccurate location in the geospatial data set.

3.2 Geographical extents of analyses

Due to the many different geospatial datasets included in this study, spatial analyses were performed within the extents of several datasets. Figure 3-2 shows all the geospatial datasets within which spatial correlations for pipeline damage in Christchurch were performed, including:

- LIQ zone of observed liquefaction effects, as described in Section 2.4;
- LiDAR Zone which is the geographical extent of LiDAR surveys in Christchurch before and after the 22 February 2011 earthquake; and
- TOT zone, which is the urban flat land area of Christchurch.

It is noted that the extent of the regional LSN liquefaction vulnerability model (discussed in Section 2.7) is covered by the TOT Zone. In addition to the above zones, pipeline damage statistics and correlations were performed in the areas within the TOT Zone but excluding the LIQ Zone in order to investigate the statistics and correlations of pipeline damage in the zones where liquefaction effects were not observed (referred to as the NOLIQ Zone). It is noted that liquefaction might have occurred in the NOLIQ Zone during the 22 February 2011 earthquake but without any observable surface manifestation.

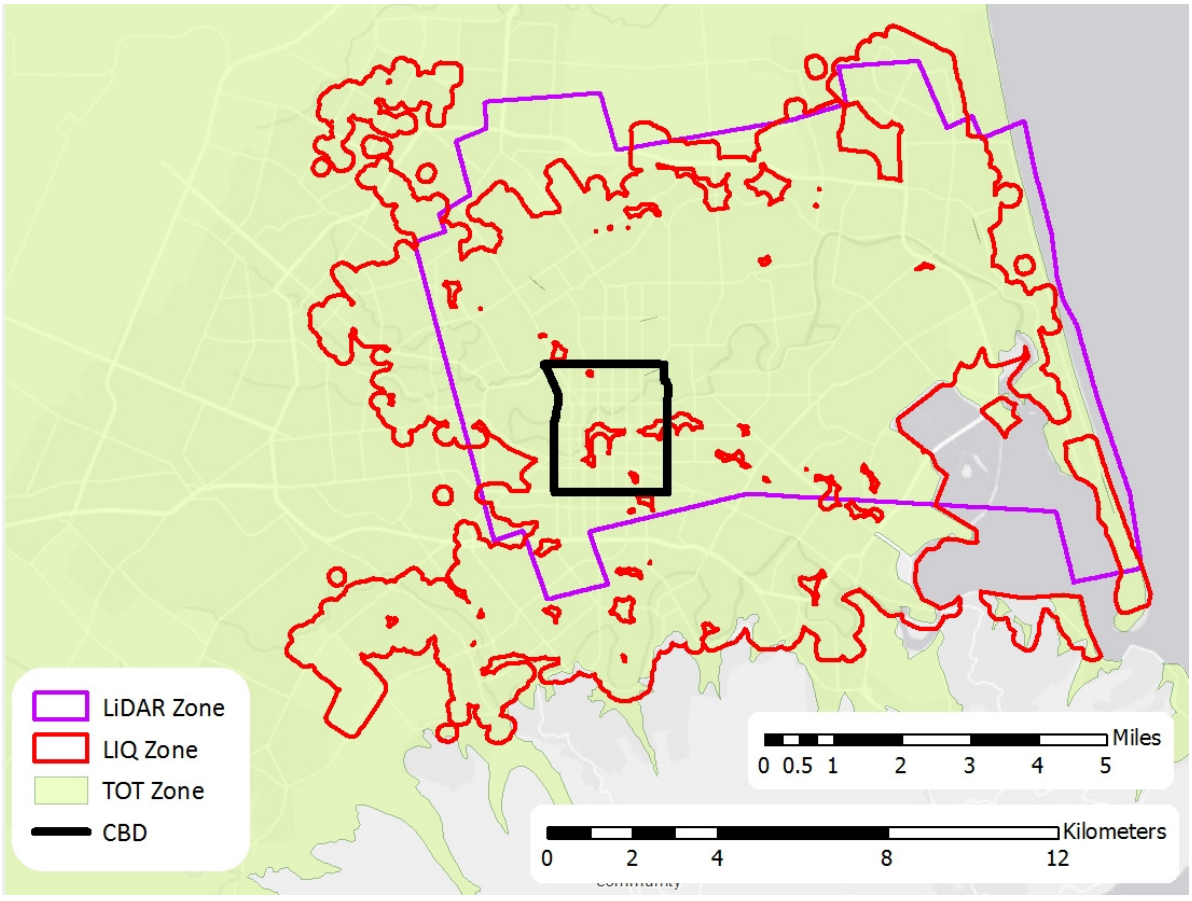

Figure 3-2 Geographical extents of different zones from which correlations are developed.

3.3 Comparison of pipeline damage correlations with lateral displacements derived from different LiDAR and satellite imagery

In addition to the comparison of liquefaction-related lateral displacements derived from unfiltered LiDAR, filtered LiDAR, and satellite imagery shown in Figure 2-13 and discussed in Section 2.6.2, a comparative study was also performed on the basis of RR correlations with lateral displacements derived from unfiltered and filtered LiDAR and satellite imagery over the geographical extent of the SAT Zone which contains all three types of data sets. The results are presented in Figure 3-3 for the three major pipe types in the water supply system, i.e., AC, CI and PVC pipes. Similar trends in RR vs lateral displacement are shown for AC pipes among all three types of data sets, whereas there are some distinctive differences for CI and PVC pipes. Overall, filtered LiDAR and satellite imagery seem to provide stronger correlations of RR with lateral displacement than unfiltered LiDAR data sets, with reasonably increasing trends of RR towards larger values of lateral displacement. It is noted that none of the RR trends shown in Figure 3-3 has an intercept at zero or very small lateral displacements, indicating that pipeline damage is also controlled by other ground surface deformation mechanisms such as liquefaction-related settlement and transient ground surface deformations due to seismic ground shaking.

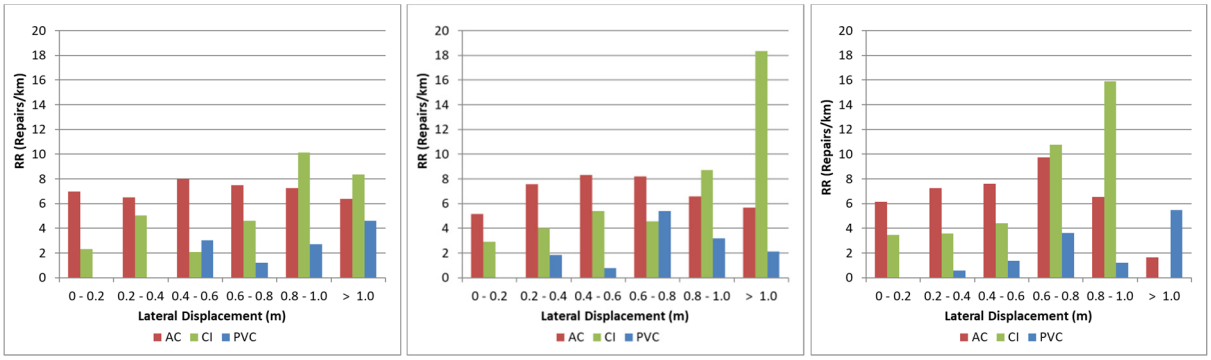

(a) (b) (c)

Figure 3-3 Histograms of AC, CI, PVC: RR vs liquefaction-related lateral ground surface displacement derived from a) unfiltered LiDAR data, b) filtered LiDAR data, and c) satellite imagery data, within the geographical extent of the SAT Zone.

The liquefaction-related filtered LiDAR lateral displacements were used in this study to investigate correlations of pipeline damage with liquefaction-induced lateral movements because of the noise in the unfiltered LiDAR data set and the stronger RR correlations with lateral displacement using filtered LiDAR and satellite imagery. As indicated previously, the satellite imagery covers a significantly smaller extent of the Christchurch area, thus restraining subsequent analyses to a much smaller geographic extent.

3.4 Statistical analysis of pipeline damage

Repairs and pipelines located in the TOT Zone, the LIQ Zone and the NOLIQ Zone were geospatially correlated with GMPGV, lateral displacement and settlement derived from filtered LiDAR data to investigate the distribution of the water supply network and pipeline damage during the 22 February 2011 earthquake as a whole, within the zone of observed liquefaction effects, and the areas outside this zone, respectively. Sections 3.4.1 through 3.4.4 present the results of the statistical analyses.

3.4.1 Comparison of RR in the NOLIQ zone and the LIQ zone

Comparative results of pipeline damage due to the 22 February 2011 earthquake (expressed as RR) for different types of pipe, age and diameter inside and outside the LIQ zone (LIQ Zone and NOLIQ Zone respectively) are presented in Tables 3-1 to 3-4. A green-to-red colour scale is used for each cell, indicating the range from the lowest to the highest values of RR, respectively. It is noted that pipelines and pipe repairs in the Port Hills area were excluded from this analysis because pipeline damage was caused by non-liquefaction-related permanent ground surface deformations (PGD) and ground failure mechanisms such as landslides and rock falls (Bouziou, 2015). RR values corresponding to pipeline lengths less than 5km were not included in Table 3-1 through Table 3-4.

Table 3-1 Pipe repair rate by year of installation for AC, CI, PVC, UPVC and MPVC pipelines located within the LIQ zone.

Year Laid	Repair Rate (Repairs/km)				
	AC	CI	PVC	UPVC	MPVC
< 1940	-	1.5	-	-	-
1940-1950	3.9	1.2	-	-	-
1950-1960	3.7	2.0	-	-	-
1960-1970	1.7	1.0	-	-	-
1970-1980	1.8	1.7	-	-	-
1980-1990	1.3	1.2	0.6	-	-
1990-2000	-	-	0.5	0.3	0.0
2000-2011	-	-	0.5	0.1	0.3
All <1940 - 2011	**2.0**	**1.6**	**0.5**	**0.2**	**0.3**

Table 3-2 Pipe repair rate by diameter for AC, CI, PVC, UPVC and MPVC pipelines located within the LIQ zone.

Diameter (mm)	Repair Rate (Repair/km)				
	AC	CI	PVC	UPVC	MPVC
50-100	-	-	-	-	-
100-150	2.6	1.5	0.9	0.2	0.3
150-200	1.6	1.6	0.3	0.0	0.3
200-250	1.6	1.9	0.1	-	0.3
250-300	-	-	-	-	-
300-350	0.7	-	0.3	-	-
350-400	-	-	-	-	-
400-450	-	-	-	-	-
450-500	-	-	-	-	-
500-550	-	-	-	-	-
550-600	-	-	-	-	-
All 50 - 600	**2.0**	**1.6**	**0.5**	**0.2**	**0.3**

Table 3-3 Pipe repair rate by year of installation for AC, CI, PVC, UPVC and MPVC pipelines located in the NOLIQ zone.

Year Laid	Repair Rate (Repairs/km)				
	AC	CI	PVC	UPVC	MPVC
< 1940	-	-	-	-	-
1940-1950	0.8	-	-	-	-
1950-1960	0.4	0.3	-	-	-
1960-1970	0.2	-	-	-	-
1970-1980	0.1	-	-	-	-
1980-1990	0.5	-	0.0	-	-
1990-2000	-	-	0.1	0.1	-
2000-2011	-	-	0.0	0.0	-
All <1940 - 2011	**0.3**	**0.3**	**0.1**	**0.04**	**-**

Table 3-4 Pipe repair rate by diameter for AC, CI, PVC, UPVC and MPVC pipelines located in the NOLIQ zone.

Diameter (mm)	Repair Rate (Repair/km)				
	AC	CI	PVC	UPVC	MPVC
50-100	-	-	-	-	-
100-150	0.3	0.3	0.0	0.1	-
150-200	0.2	0.3	0.0	0.1	-
200-250	0.2	0.3	0.1	0.0	-
250-300	0.0	-	-	-	-
300-350	0.3	-	0.1	-	-
350-400	-	-	-	-	-
400-450	-	-	-	-	-
450-500	-	-	-	-	-
500-550	-	-	-	-	-
550-600	-	-	-	-	-
All 50 - 600	**0.3**	**0.3**	**0.1**	**0.04**	**-**

As shown in Tables 3-1 to 3-4, the highest RRs overall are attributed to AC pipes, followed by CI pipes. Pipes consisting of PVC-based materials sustained the lowest levels of damage both within the LIQ Zone as well as outside of the LIQ Zone. Comparing Tables 3-1 to 3-2 with Tables 3-3 to 3-4, the RR is 5 to 6.7 times higher in the LIQ Zone compared to the NOLIQ Zone, highlighting the dominant effects of liquefaction in pipeline damage over other effects such as transient ground deformations (TGD).

Note that the RR in Tables 2-6 and 2-7 are for the TOT Zone and hence the values are between the higher RR values for the LIQ zone (Tables 3-1 and 3-2) and the lower RR for the NOLIQ zone (Tables 3-3 and 3-4).

3.4.2 Statistical analysis with respect to GMPGV

Figure 3-4 to 3-6 show histograms of repairs, pipeline length and RR for the three major pipe types in the water supply system (i.e., AC, CI and PVC pipes) vs GMPGV using the geographical extents of the TOT Zone, the NOLIQ Zone and the LIQ zone. Comparison of the distributions of repairs in Figure 3-4a, 3-5a and 3-6a with respect to GMPGV indicates that the majority of repairs (more than an order of magnitude of the total number of repairs) is located within the LIQ zone even though, as shown in Figures 3-4b, 3-5b and 3-6b, pipelines are approximately equally distributed between the LIQ and NOLIQ zones.

The results in Figures 3-4c, 3-5c and 3-6c of RR vs GMPGV show that the highest RR values are related to pipeline damage within the LIQ zone, whereas the maximum RRs in the areas not affected by liquefaction (NOLIQ zone) are slightly higher than 1 repair/km.

It is noted that the increasing trends of RR with respect to GMPGV in Figure 3-5c for AC and CI pipelines in the NOLIQ zones are in very good agreement with the correlations of RR vs GMPGV developed by Bouziou (2015).

Pipelines within the LIQ Zone were subjected both to transient ground surface deformation effects and to liquefaction-related deformations. The highest levels of ground shaking in Figure 2-8, reflected by GMPGV, more or less overlap with the LIQ Zone. In addition to pipeline damage caused by ground shaking within the LIQ Zone, there was damage caused by liquefaction effects.

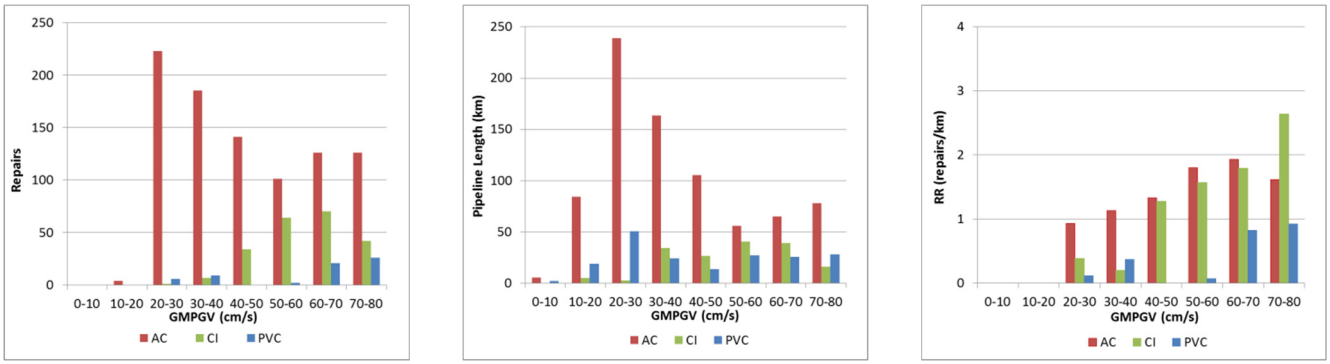

(a) **(b)** **(c)**

Figure 3-4 Histograms of AC, CI, PVC within the TOT zone: a) Repairs vs GMPGV, b) Pipeline length vs GMPGV, c) RR vs GMPGV.

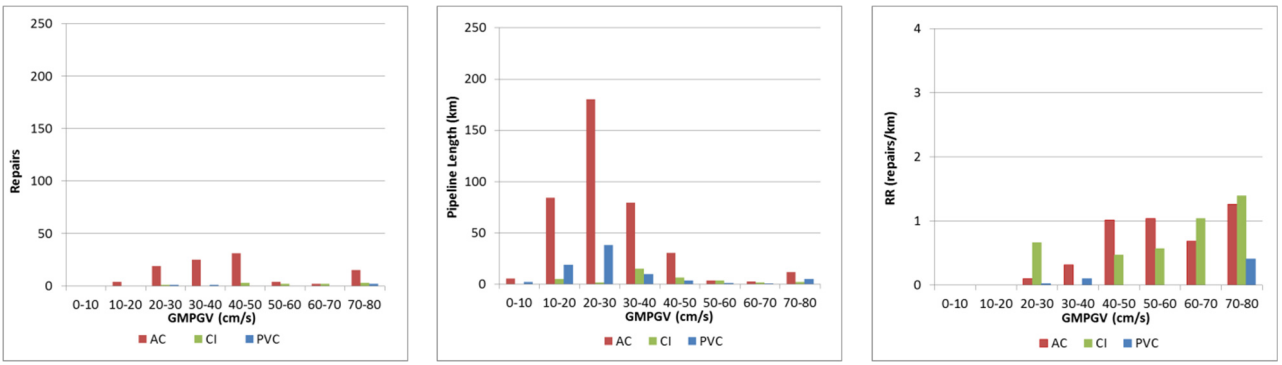

(a) **(b)** **(c)**

Figure 3-5 Histograms of AC, CI, PVC within the NOLIQ zone: a) Repairs vs GMPGV, b) Pipeline length vs GMPGV, c) RR vs GMPGV.

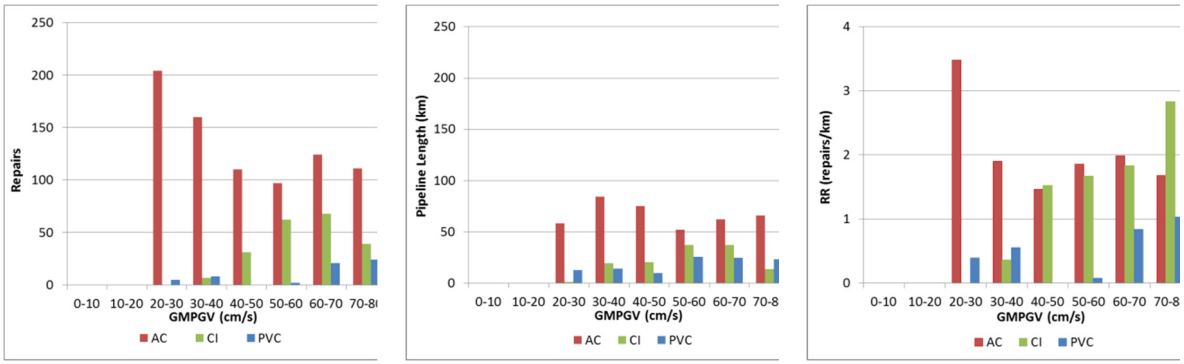

(a) (b) (c)

Figure 3-6 Histograms of AC, CI, PVC within the LIQ zone: a) Repairs vs GMPGV, b) Pipeline length vs GMPGV, c) RR vs GMPGV.

3.4.3 Statistical analysis with respect to settlement

Figures 3-7 to 3-9 show histograms of repairs, pipeline length and RR for the three major pipe types in the water supply system (i.e., AC, CI and PVC pipes) vs settlement using the geographical extents of the TOT Zone, the NOLIQ Zone and the LIQ zone.

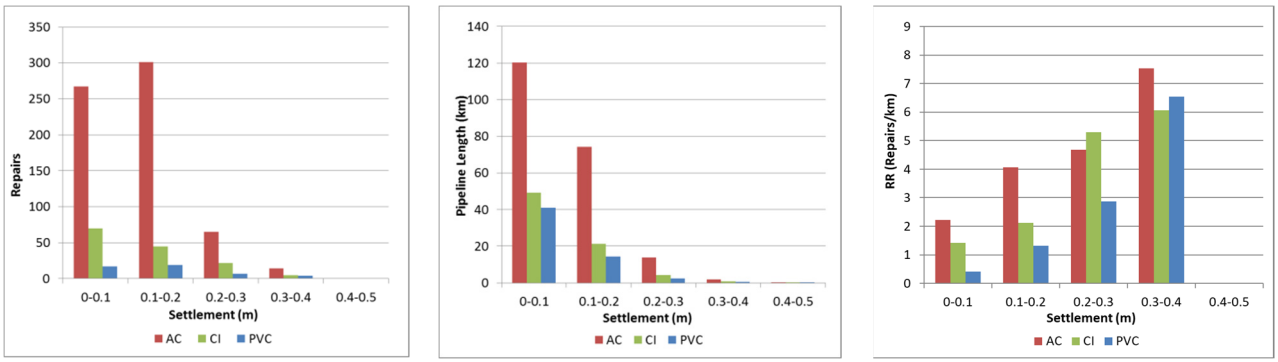

(a) (b) (c)

Figure 3-7 Histograms of AC, CI, PVC within the TOT zone: a) Repairs vs Settlement, b) Pipeline length vs Settlement, c) RR vs Settlement.

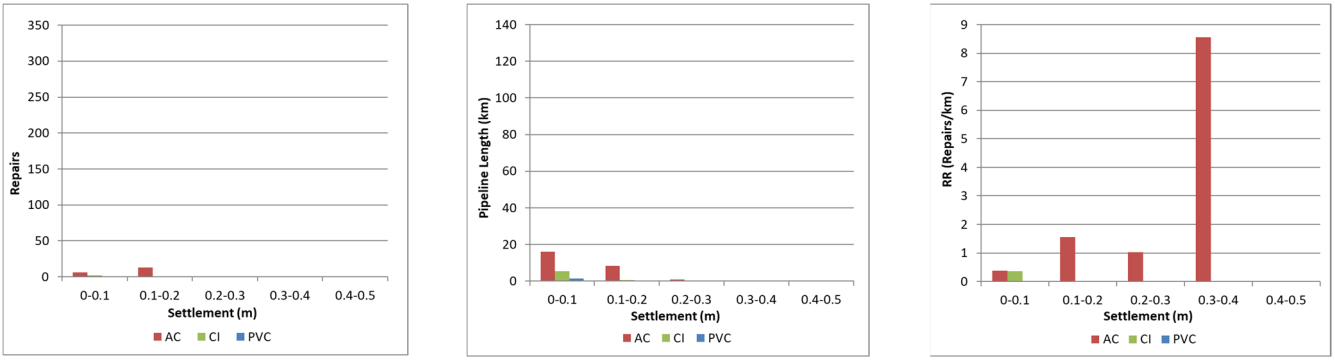

(a) **(b)** **(c)**

Figure 3-8 Histograms of AC, CI, PVC within the NOLIQ zone: a) Repairs vs Settlement, b) Pipeline length vs Settlement, c) RR vs Settlement.

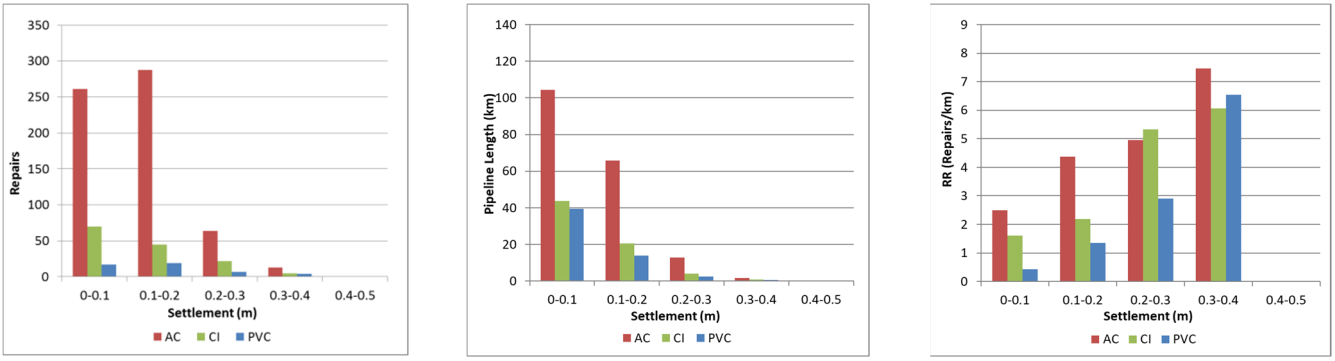

(a) **(b)** **(c)**

Figure 3-9 Histograms of AC, CI, PVC within the LIQ zone: a) Repairs vs Settlement, b) Pipeline length vs Settlement, c) RR vs Settlement.

As previously discussed, settlement values were derived from LiDAR datasets collected before and after the 22 February 2011 earthquake and were corrected for tectonic movement to reflect settlement caused by liquefaction effects. It is noted that liquefaction-related settlement may have also taken place during the 22 February 2011 earthquake in the NOLIQ areas without any surface manifestation, and may have also contributed to pipeline damage.

As shown in Figure 3-7 to 3-9, most of the pipeline repairs and most of AC, CI and PVC pipelines are located within the LIQ Zone. Figure 3-9c demonstrates that RR values greater than zero are related to very small to negligible settlement, indicating that other effects such as liquefaction-induced lateral ground strain and ground shaking have also contributed to pipeline damage within the LIQ Zone. As previously discussed, pipelines within the LIQ

Zone were subjected both to transient ground surface deformation effects and to liquefaction-related deformations.

3.4.4 Statistical analysis with respect to lateral displacement

Figure 3-10 through 3-12 show histograms of repairs, pipeline length and RR for the three major pipe types in the water supply system (i.e. AC, CI and PVC pipes) vs lateral displacement using the geographical extents of the TOT Zone, the NOLIQ Zone and the LIQ zone. As previously discussed, lateral displacements were derived from filtered LiDAR datasets collected before and after the 22 February 2011 earthquake and were corrected for tectonic movement to reflect lateral displacement caused by liquefaction effects. Similar to the liquefaction-related settlement, liquefaction-related lateral displacement may have also taken place during the 22 February 2011 earthquake in the NOLIQ Zone without any surface manifestation and may have also contributed to pipeline damage in the wider TOT Zone.

As shown in Figure 3-10 through Figure 3-12 most of the pipe repairs and most of AC, CI and PVC pipes are located within the TOT zone, and the highest RR values are related to damage within the LIQ zone. RR values as high as 2 repairs/km in Figure 3-12c are observed at very small to negligible lateral displacement, indicating that pipeline damage was caused by some combination of liquefaction-induced settlement and ground shaking.

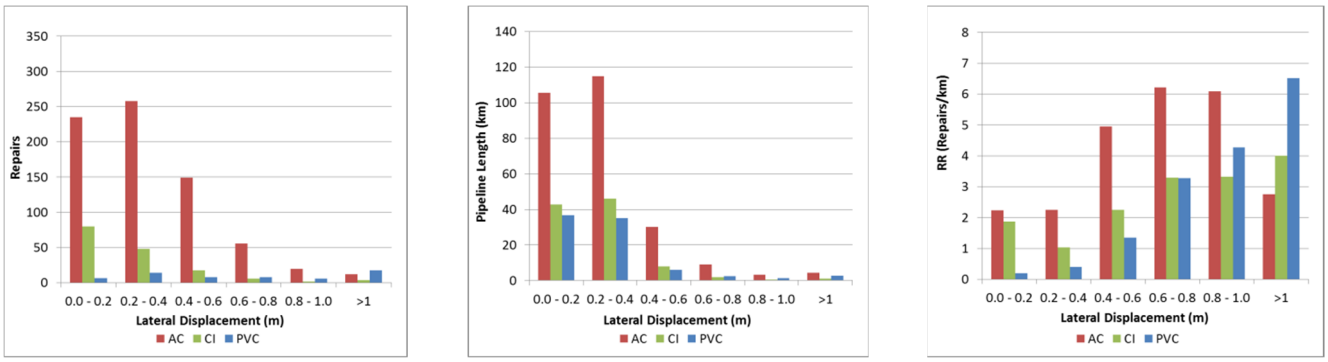

(a) **(b)** **(c)**

Figure 3-10 Histograms for AC, CI, and PVC pipelines within the TOT zone for: a) repairs, b) pipeline length, and c) repair rate vs lateral displacement.

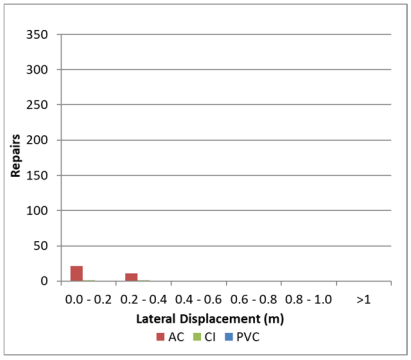

(a)

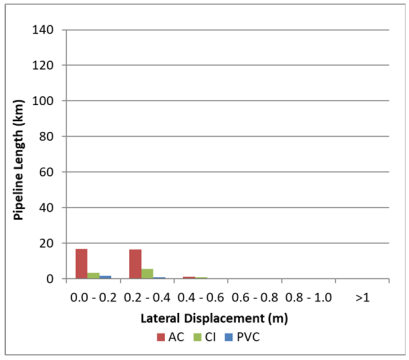

(b)

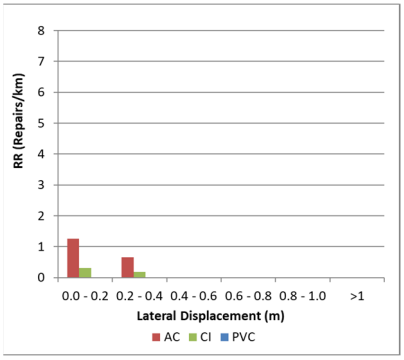

(c)

Figure 3-11 Histograms of AC, CI, and PVC pipelines within the NOLIQ zone for: a) repairs, b) pipeline length, c) repair rate vs lateral displacement.

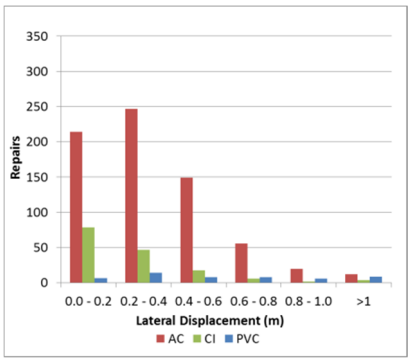

(a)

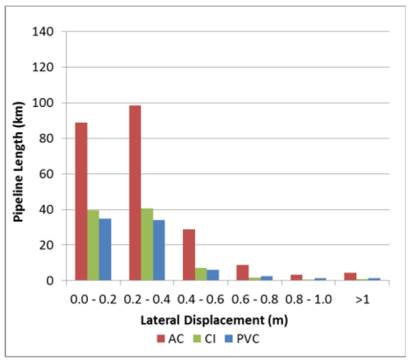

(b)

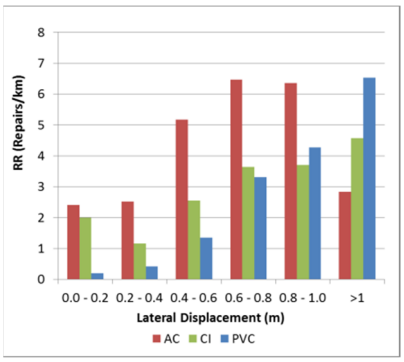

(c)

Figure 3-12 Histograms of AC, CI, and PVC pipelines within the LIQ zone for: a) repairs, b) pipeline length, c) repair rate vs lateral displacement.

3.4.5 RR correlations of pipeline damage with the combined liquefaction-induced lateral displacement and settlement

Similar to the procedure developed by Boscardin and Cording (1989) for masonry and timber buildings subject to underground construction and mining-induced ground movements, and similar to RR correlations with both lateral ground surface strain and differential ground surface movement developed by Bouziou (2015), the simultaneous effects of liquefaction-related settlement and lateral movement were combined in RR correlations to have an improved representation of liquefaction-induced pipeline damage during the 22 February 2011 earthquake.

Lateral displacements from the filtered LiDAR data sets at 4m spacing and settlements from the filtered LiDAR data sets at 5m spacing were used in these RR correlations. Pipelines and repairs were spatially intersected with lateral displacement and settlement within the TOT Zone, and RR was calculated for a given pair of lateral displacement and settlement interval by dividing the number of repairs for a particular type of pipeline by the kilometres of that pipeline type within the same pair of intervals. The interval for lateral displacement was 0.2m, and for settlement was 0.1m. The RRs were associated with the appropriate pair of lateral displacement and settlement and were used as data points for RR correlations. The screening criterion described by Bouziou (2015) was applied for each set of data points to ensure fidelity in RR correlations. The confidence interval is relaxed at 80% and 70% for AC and CI pipelines, respectively, in order to produce as many reliable data points as possible and cover the broadest range of ground movements.

The resulting RR correlations for AC and CI pipes are presented as contour plots of RR in the 2-D space defined by lateral displacement and settlement in Figure 3-13. There was not enough data for polynomial interpolations to produce meaningful contour plots of RR vs lateral displacement and settlement for PVC pipelines.

The global polynomial interpolation method in ArcMap 10.1 (2018) was used to fit a smooth surface of RR contours as illustrated in Figure 3-13. A first-order polynomial model was applied to the data. The resulting contour surfaces are presented in Figures 3-13a and 3-13b for AC and CI pipelines, respectively. The extent of lateral displacement and settlement over which there are statistically relevant CI RRs is smaller than the extent of same for AC pipelines. This difference is related to the significantly higher number of AC pipeline repairs and their wider geographical distribution across Christchurch. The results in Figure 3-13 show that AC pipelines sustained higher RRs at comparable levels of lateral and vertical movement compared to CI pipelines.

It is noted that the contours for AC pipes in Figure 3-13 are not zero at the (0,0) intercept. As shown in Figure 3-5a, a large number of AC repairs is associated with GMPGV values between 20cm/s and 40cm/s. These GMPGV values and AC repairs are mainly identified outside the LIQ zone (see Figure 3-5). Moreover, as shown in Figure 3-5c, GMPGV values between 20cm/s and 40cm/s are associated with high RR levels for AC pipelines. These AC repairs are not associated with liquefaction-induced lateral displacement and settlement. Nevertheless, they fall within the TOT Zone and, thus, are included in the correlation shown in Figure 3-13. It appears, therefore, that GMPGV contributes to AC pipeline damage when the lateral displacement and settlement shown in Figure 3-13a are negligible.

GMPGV does not have the same effect on pipeline damage for CI pipelines as it does for AC pipelines in the TOT Zone, as shown in Figure 3-13b. This observation is corroborated by RR correlations with GMPGV developed by Bouziou (2015) that show AC pipelines being more susceptible to GMPGV damage than CI pipelines.

Comparison between Figure 3-13a and Figure 3-13b shows that AC pipelines are more susceptible to damage caused by lateral displacement than CI pipelines. In contrast, CI pipelines seem to be more susceptible to damage due to settlement.

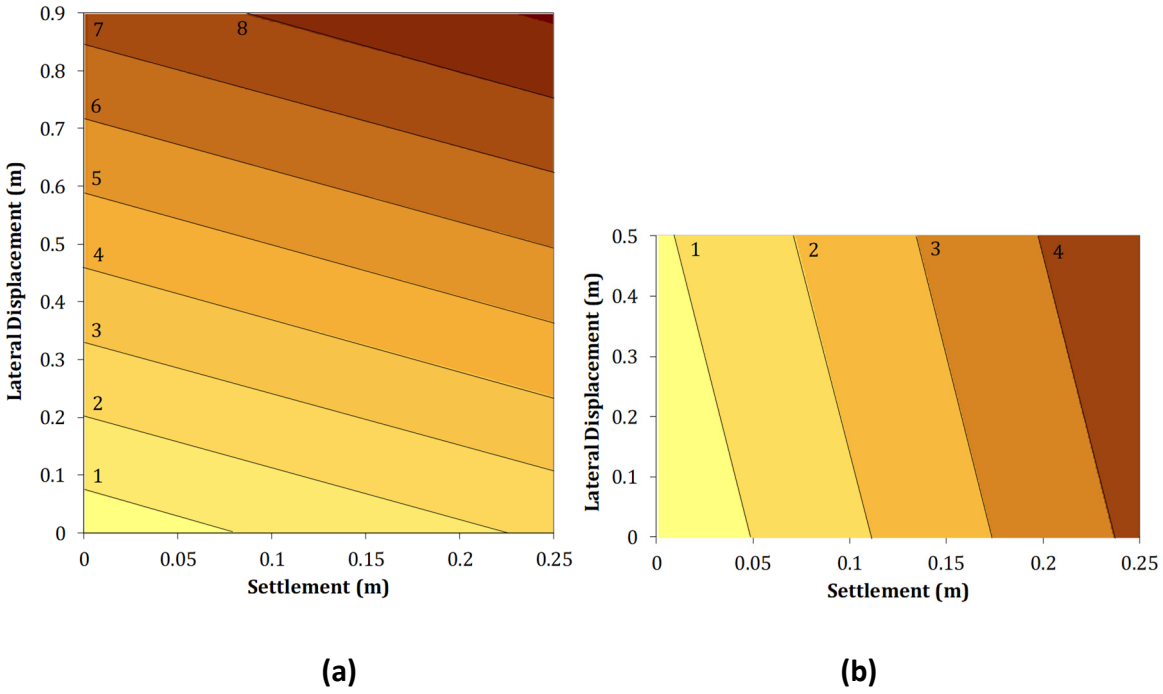

Figure 3-13 Correlations of RR with lateral displacement and settlement: a) AC and b) CI pipes within the TOT Zone.

3.4.6 Correlations between pipeline damage and LSN

Similar to the previous statistical analyses of pipeline damage presented herein, statistical analysis was also performed to investigate pipeline damage, expressed as RR, during the 22 February 2011 earthquake with respect to the CPT-based liquefaction vulnerability index parameter LSN. The LSN wide area model described in Section 2.7 was used to correlate pipe repairs and pipeline lengths within the water supply network pertaining to the 22 February 2011 earthquake with the 50th and 75th percentile values of LSN in each SEGP across Christchurch.

The distribution of repairs, pipeline length and RR with respect to the 50th and 75th values of LSN for AC, CI and PVC pipelines is shown in Figure 3-14 and Figure 3-15. Overall, AC pipelines are more vulnerable with respect to any level of LSN than CI pipelines, and CI pipelines in most cases are more vulnerable with respect to LSN than PVC pipelines. The histograms of RR with respect to the 75th percentile LSN values provide stronger increasing trends than the histograms of RR with respect to the 50th percentile LSN values.

It is noted that the pipeline RRs shown in Figure 3-14 and Figure 3-15 are greater than zero at LSN=0. Similar to RR correlations with the liquefaction-induced ground displacements

presented in Sections 3.4.1 through 3.4.5, TGD effects, expressed in this study through GMPGV, appear to influence pipeline damage, when liquefaction vulnerability, expressed through LSN, is zero.

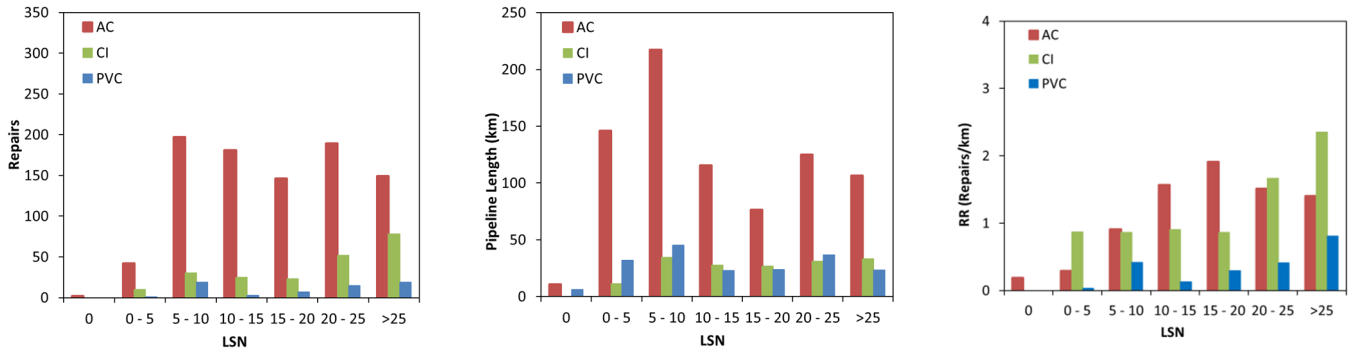

(a) **(b)** **(c)**

Figure 3-14 Histograms of: a) Repairs, b) Pipeline Length, and c) RR vs LSN (50th percentile), for AC, CI, PVC within the TOT zone.

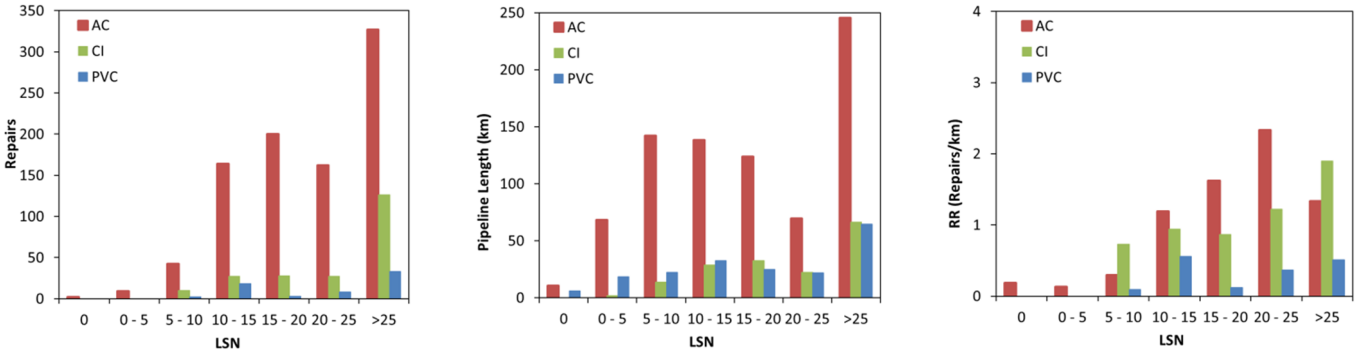

(a) **(b)** **(c)**

Figure 3-15 Histograms of: a) Repairs, b) Pipeline Length, and c) RR vs LSN (75th percentile), for AC, CI, PVC within the TOT zone.

4 Development of pipe repair rate functions

4.1 Methodology for assessing the additional pipeline damage caused by liquefaction-induced effects

As discussed in the previous sections, pipeline damage in liquefied areas is primarily attributed to liquefaction effects (i.e., lateral and vertical ground displacements and deformations). TGD also have a contributing effect and thereby affect the fragility functions particularly at small vertical and horizontal ground movements and low LSN values. Therefore, it is useful to remove the damage caused by the TGD effects so that the fragility functions can be expressed as the repair rate of additional damage caused by liquefaction effects ($RR_{Add\text{-}Liq}$) in addition to the base repair rate caused by TGD (RR_{TGD}).

$$RR = RR_{TGD} + RR_{Add-Liq} \quad (4\text{-}1)$$

4.1.1 Estimating the GMPGV breaks and RR_{TGD}

Pipeline damage (i.e., pipe repairs in this study) attributed to seismic wave effects, or TGD, was estimated by RR vs GMPGV correlations developed by Bouziou (2015). These correlations are for pipeline repairs outside the LIQ Zone after the 22 February 2011 earthquake and are in close agreement with the RR correlations for the NOLIQ zone shown in Figure 3-5c.

To estimate the RR_{TGD} for AC and CI pipes in the TOT Zone, the GMPGV for each pipe segment was estimated using the contour map of GMPGV illustrated in Figure 2-8. For each bin of GMPGV (intervals had a 10 cm/s range of values), the expected value RR_{TGD} was estimated for AC and CI pipelines using the RR vs GMPGV correlations. Having calculated the total length of pipelines within each GMPGV interval in the TOT Zone, and having an estimate of RR_{TGD} for the same GMPGV interval, the expected number of repairs attributed to the specific GMPGV interval was calculated within the TOT Zone. These repairs, and the consequent RR_{TGD}, represent pipeline damage that would likely have occurred if liquefaction would not have occurred.

Based on the very low levels of RR_{TGD} with respect to GMPGV shown in Figure 3-5c for PVC pipelines in the NOLIQ zone, it was assumed that RR = $RR_{Add\text{-}Liq}$ for PVC pipelines. That is, the additional amount of pipeline damage for PVC pipelines due to liquefaction effects is equivalent to the pipeline damage that was actually recorded.

4.1.2 Adjusting the repair rate vs combined vertical and lateral displacements

The additional number of repairs caused by liquefaction and the pipelines in the TOT area were correlated with lateral displacements and settlement derived from filtered LiDAR data collected before and after the 22 February 2011 earthquake to develop correlations of the additional repair rate, $RR_{Add\text{-}Liq}$, with lateral displacement and settlement with the same methodology described in Section 3.4.5. As previously discussed, lateral displacements from the filtered LiDAR data sets at 4m spacing and settlements from the filtered LiDAR data sets at 5m spacing were used in these $RR_{Add\text{-}Liq}$ correlations. The interval for lateral displacement was 0.2m, and for settlement was 0.1m. Similar to the correlations presented in Section 3.4.5, the screening criterion described by Bouziou (2015) was applied for each set of data points and the confidence interval was relaxed at 80% and 70% for AC and CI pipelines, respectively, in order to produce as many reliable data points as possible and cover the broadest range of ground movements.

The resulting $RR_{Add\text{-}Liq}$ correlations for AC and CI pipelines are presented as contour plots of RR in the 2-D space defined by lateral displacement and settlement in Figure 4-1. The contour plots in Figure 3-13 and Figure 4-1 show a small shift in the contours such that the $RR_{Add\text{-}Liq}$ in Figure 4-1 is almost zero at the (0,0) intercept (i.e., when settlement and lateral displacement are zero, then $RR_{Add\text{-}Liq}$ should be zero).

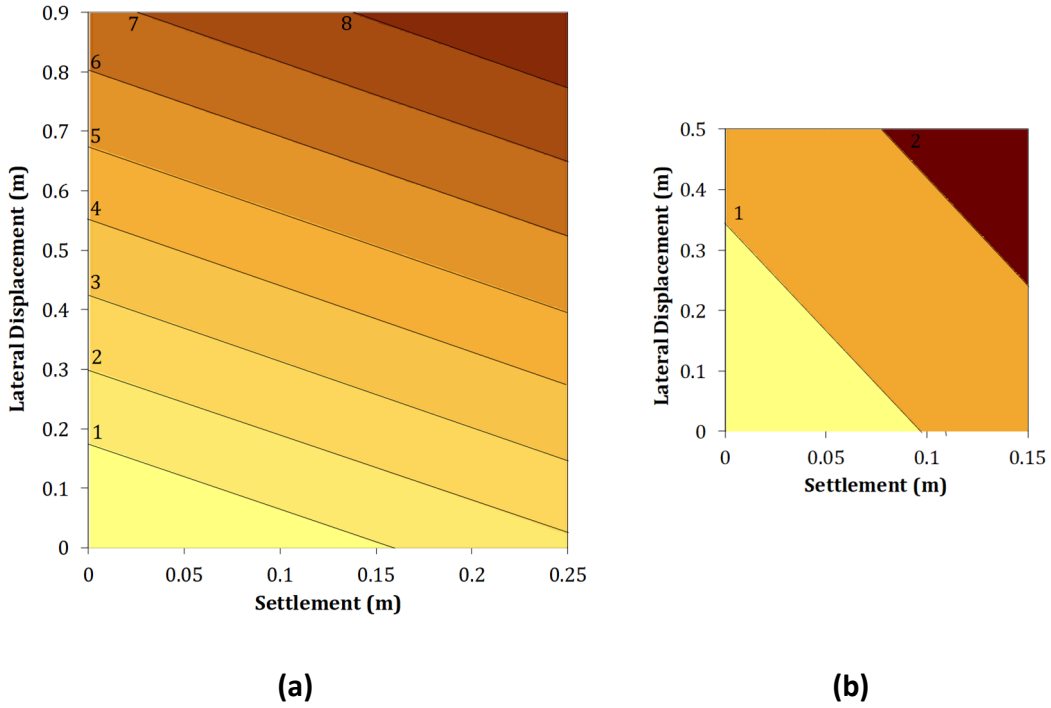

Figure 4-1 Correlations of $RR_{Add\text{-}Liq}$ with lateral displacement and settlement: a) AC and b) CI pipes within the TOT Zone.

4.1.3 Adjusting the repair rate vs LSN

Similar to the statistical analysis of pipeline damage with respect to LSN presented in Section 3.4.6, correlations of pipeline damage were performed with LSN for the three major pipe types, i.e., AC, CI and PVC pipes, using the estimated additional repair rate due to liquefaction-effects, $RR_{Add\text{-}Liq}$. Similar to the process described in Section 3.4.6, the LSN wide area model was used to correlate the additional number of pipe repairs due to liquefaction and pipelines pertaining to the 22 February 2011 earthquake within the TOT Zone with the 50^{th} and 75^{th} percentile values of LSN across Christchurch.

Correlations of $RR_{Add\text{-}Liq}$ with respect to the 50^{th} and 75^{th} LSN values for AC, CI and PVC pipelines are presented in Figure 4-2. The histograms of $RR_{Add\text{-}Liq}$ presented in Figure 4-2 are smaller than the RR shown in Figures 3-14 and 3-15. The $RR_{Add\text{-}Liq}$ correlations are close to zero at an LSN value of zero (i.e., when the predicted liquefaction vulnerability is zero, then $RR_{Add\text{-}Liq}$ should be zero).

The results also show that AC pipelines are more susceptible to liquefaction-related effects than CI pipelines, and CI pipes are more susceptible to liquefaction-related effects than PVC pipes.

The histograms of $RR_{Add\text{-}Liq}$ with respect to the 75^{th} percentile LSN values provide stronger increasing trends than the histograms of $RR_{Add\text{-}Liq}$ with respect to the 50^{th} percentile LSN values. The correlation of pipeline damage with the 75^{th} percentile LSN values therefore produces a better-defined trend of increasing $RR_{Add\text{-}Liq}$ vs LSN. Indicative, smoothed trend lines have been visually fitted to the 75^{th} percentile LSN histograms and are shown in Figure 4-3. These are indicative lines only to depict the shape of the $RR_{Add\text{-}Liq}$ vs LSN functions. Further work is necessary to more robustly fit $RR_{Add\text{-}Liq}$ vs LSN functions to the data.

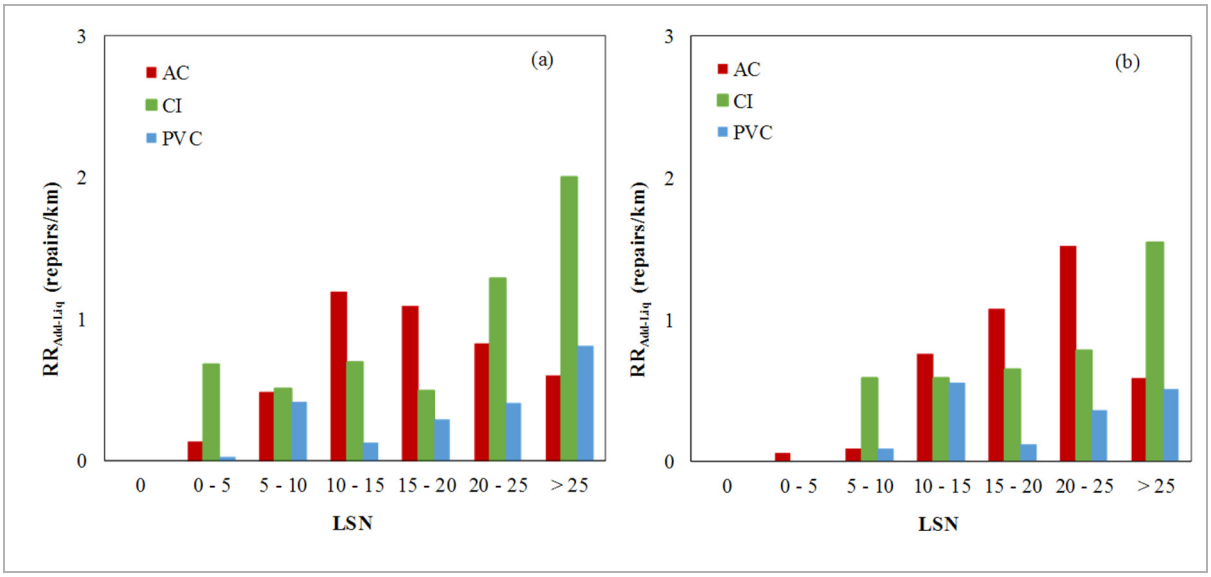

(a) **(b)**

Figure 4-2 Histograms of $RR_{Add\text{-}Liq}$ vs LSN within the TOT Zone for: a) AC, CI and PVC pipelines using the 50th percentile, and b) AC, CI and PVC pipelines using the 75th percentile.

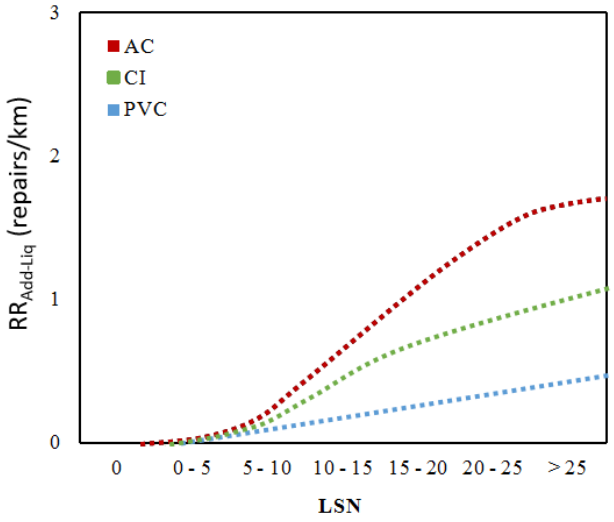

Figure 4-3 Indicative $RR_{Add\text{-}Liq}$ vs LSN functions for AC, CI and PVC pipelines based on 75th percentile calculated LSN values.

5 Application

The correlations developed in this study can be used for both estimating pipeline damage following an earthquake and also for developing predictive models for pipeline damage in areas with liquefaction susceptible soils. Figure 5-1 outlines how the correlations can be used for pipeline damage modelling from potential earthquake scenarios in areas affected by the combined effects of liquefaction and seismic ground shaking. Such assessments can then inform system performance studies and also loss modelling. In this case, input parameters, such as CPT-based LSN values, combined with seismic ground motion prediction models, are used to predict the distribution of pipeline damage for different earthquake scenarios.

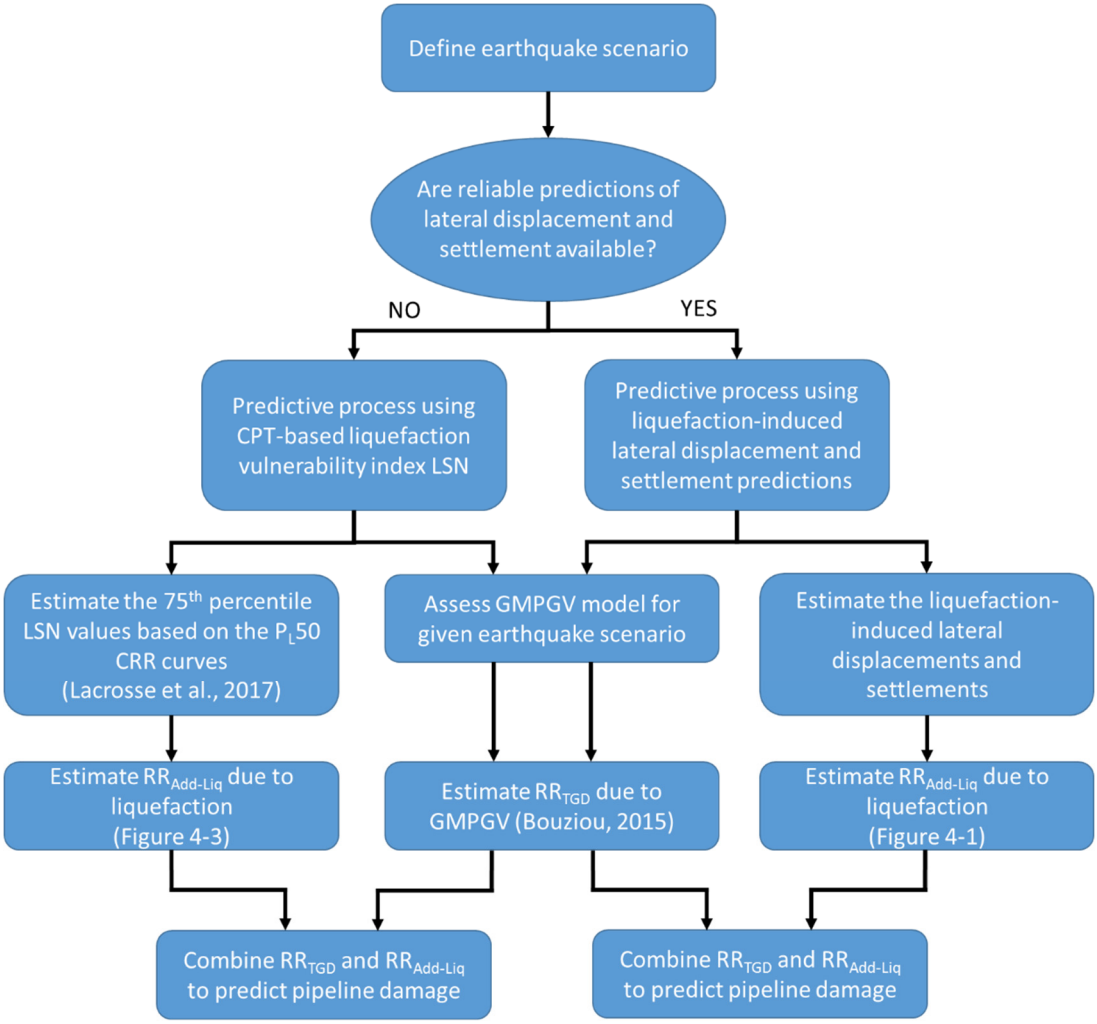

Figure 5-1 Flow chart of suggested framework for assessing pipe line damage for potential earthquake scenarios in areas affected by the combined effects of liquefaction and seismic ground shaking.

These correlations could also be incorporated into the pipeline design process where there is a performance objective of a repair rate less than a maximum accepted amount for the particular design level of earthquake shaking.

In addition to pre-event risk assessment and planning, the findings of this work can also be applied after an earthquake to improve emergency response and recovery. Using the framework in Figure 5-2 pipeline damage can be rapidly estimated using remote sensing technologies that provide information about the distribution of ground surface movements. This information guides the detailed damage assessment process and restoration of the pipeline network to enhance emergency repairs and support community recovery. The methodology can be incorporated into regional response and recovery operations.

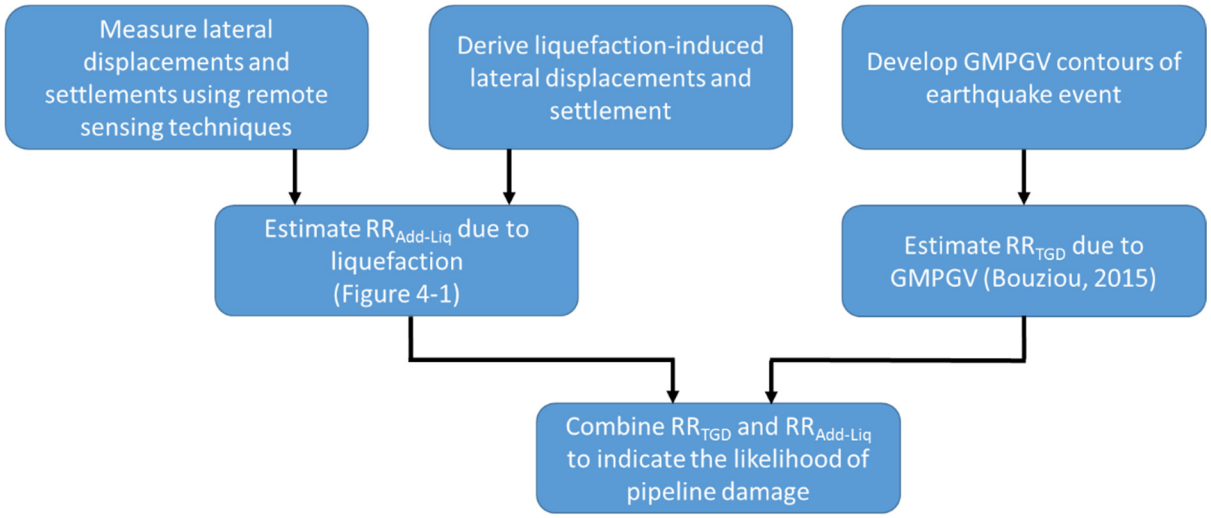

Figure 5-2 Flow chart of suggested framework for assessing the likelihood of pipeline damage for post-earthquake event situations.

References

ArcMap. (2018). [computer software], version 10. 6. Redlands, California, USA: Environmental Systems Resource Institute.

Beavan, J., Levick, S., & Lee, J. J. K. (2012). *Ground displacements and dilatational strains caused by the 2010-2011 Canterbury earthquakes*. GNS Science Consultancy Report 2012/67, Wellington, New Zealand.

Boscardin, M. D., & Cording, E.J. (1989). Building response to excavation-induced settlement. *Journal of Geotechnical Engineering*, *115(1),* 1-21.

Bouziou, D., & O'Rourke, T. D., Cubrinovski, M., & Henderson D. (2015). Evaluation of Ground Deformations during the 2010-2011 Canterbury Earthquake Sequence. *Proceedings of the 6th International Conference on Earthquake Geotechnical Engineering* Christchurch, New Zealand. Retrieved from http://www.6icege.com/

Bouziou, D. (2015). *Earthquake-induced ground deformation effects on buried pipelines.* (PhD Thesis). Cornell University, Ithaca NY, USA.

Bouziou, D., & O'Rourke, T.D. (2015). Water Distribution System Response to the 22 February 2011 Christchurch Earthquake. *Proceedings of the 6th International Conference on Earthquake Geotechnical Engineering*, Christchurch, New Zealand. Retrieved from http://www.6icege.com/

Bradley, B., & Hughes, M. (2013). *Conditional peak ground accelerations in the Canterbury earthquakes for conventional liquefaction assessment* (Technical Report Part 2), prepared for the Ministry of Business, Innovation and Employment, Wellington, New Zealand.

Canterbury Geotechnical Database. (2012). *LiDAR and digital elevation models, map layer CGD0500 - 23 July 2012*. Retrieved from https://canterburygeotechnicaldatabase.projectorbit.com/.

Canterbury Geotechnical Database. (2013). *Liquefaction interpreted from aerial photography, map layer CGD0200 - 11 Feb 2013*. Retrieved from https://canterburygeotechnicaldatabase.projectorbit.com/.

Christchurch City Council. (2010). *Infrastructure Design Standard*. Christchurch, New Zealand: Author.

Community and Public Health. (2016). *Drinking Water*. Christchurch, New Zealand: Canterbury District Health Board.

Cubrinovski, M., Hughes, M., Bradley, B., McCahon, I., McDonald, Y., Simpson, H., Cameron, R., Christison, M., Henderson, B., Orense, R., & O'Rourke, T. (2011). *Liquefaction impacts on pipe networks*. Recovery Project No. 6, Natural Hazards Research Platform, Christchurch, New Zealand: University of Canterbury.

Cubrinovski, M., Hughes, M., Bradley, B., Noonan, J., Hopkins, R., McNeil, S., English, G. (2014). *Performance of horizontal infrastructure in Christchurch city through the 2010-2011 Canterbury Earthquake Sequence*. (Research Report 2014-02)., Christchurch, New Zealand: Civil & Natural Resources Engineering, University of Canterbury.

Earthquake Commission., (2011). Geonet: Processed strong ground motions. Wellington, New Zealand: Author. Retrieved from ftp://ftp.geonet.org.nz/strong/processed/Proc/2011/. [accessed June 2013].

Eideinger, P., Tang, A., O'Rourke, T. D., Baska D., Davis C., Kwasinski A. et al. (2012). Christchurch New Zealand Earthquake Sequence of Mw 7.1 September 04, 2010 Mw 6.3 February 22, 2011 Mw6.0 June 13, 2011: Lifeline Performance. *Technical Council on Lifeline Earthquake Engineering Monograph No. 40*. Reston, VA, USA.

GNS Science. (n.d.). *New Zealand Geology Web Map*. Wellington, New Zealand: Author. Retrieved from http://data.gns.cri.nz/geology/.

Idriss I. M., Boulanger R. W. (2008). *Soil liquefaction during earthquakes*. Oakland, CA, USA: Earthquake Engineering Research Institute.

Iwasaki, T., Arakawa, T., & Tokida, K. (1982). Simplified procedures for assessing soil liquefaction during earthquakes. In *Proceedings of the Conference on Soil Dynamics and Earthquake Engineering*. Southampton, UK.

Lacrosse V., van Ballegooy S., & Ogden M. (2017). Liquefaction hazard mapping – liquefaction vulnerability mapping for a given return period versus return period mapping for a given severity of liquefaction vulnerability. In *Proceedings of the 3rd Performance Based Design Conference (PBDIII)*. Vancouver, Canada.

Martin, J. G., & Rathje, E. M. (2014). Lateral spread deformations from the 2011 Christchurch, New Zealand earthquake measured from satellite images and optical image correlation. In *Proceedings of the 10th U.S. National Conference on Earthquake Engineering*. Anchorage, Alaska, USA.

Martin J. G. (2014). *Measuring Liquefaction-Induced Deformation from Optical Satellite Imagery*. (MSc Thesis). Austin, USA: University of Texas.

O'Callaghan F. W. (2014). Pipeline performance experiences during seismic events in New Zealand over the last 27 years. In *Proceedings of the 17th Plastic Pipes Conference PPXVII*. Chicago, Illinois, USA.

O'Rourke, M. J., & Liu, X. (1999). *Response of buried pipelines subject to earthquake effects, Monograph No.3*. Multidisciplinary Center for Earthquake Engineering Research, Buffalo, NY, USA.

O'Rourke T. D., Jeon, S. S., Toprak, S., Cubrinovski, M., Hughes, M., van Ballegooy, M., & Bouziou, D. (2104). Earthquake response of underground pipeline networks in Christchurch, NZ. *Earthquake Spectra, 30(1)*, 183-204.

Stronger Christchurch Infrastructure Rebuild Team. (2012). *Condition Assessment of Horizontal Infrastructure within the Central City*. (Investigation Report, Second Issue. 11 May, 2012). Christchurch, New Zealand: Author.

Tonkin + Taylor Ltd. (2015). *Canterbury Earthquake Sequence: Increased Liquefaction Vulnerability Assessment Methodology*. (Increased Liquefaction Vulnerability Report). Christchurch, New Zealand: Author.

Tonkin + Taylor Ltd. (2013). *Liquefaction vulnerability study - Report to Earthquake Commission*. (Report 52020.0200). Christchurch, New Zealand: Author.

van Ballegooy S., Wentz, F., & Boulanger, R. W. (2015). Evaluation of CPT-based liquefaction procedures at regional scale. *Soil Dynamics and Earthquake Engineering, 79*, 315-334.

van Ballegooy, S., Malan, P., Lacrosse, V., Jacka, M. E., Cubrinovski, M., Bray, J. D., O'Rourke, T., Crawford, S., & Cowan, H. (2014). Assessment of Liquefaction-Induced Land Damage for Residential Christchurch. *Earthquake Spectra, 30(1)*. 31 – 55.

Water New Zealand. (2017). *National Asbestos Cement Pressure Pipe Manual. Good Practice Guide*, 2nd Edition, Wellington, New Zealand: Author.

Spatial Correlations of Underground Pipeline Damage in Christchurch

Correlations with liquefaction-induced ground surface deformations and CPT-based liquefaction vulnerability index parameters

Primary Contact Robert Finch
Engineering Core Block
Ground Floor, Rm 138
Ph (03) 369 5152
M +64 21 567 842
E director@quakecentre.ac.nz

www.quakecentre.co.nz